The A Dependence of Open Charm and Bottom Production

R. Vogt[a,b*]

[a]Nuclear Science Division, MS 70-319
Lawrence Berkeley Laboratory,
University of California, Berkeley, California 94720

[b]Physics Department,
University of California, Davis, California, 95616

Abstract

We study inclusive heavy quark and exclusive heavy quark pair production in pp and pA interactions. Intrinsic transverse momentum is introduced in pp interactions. Nuclear effects are introduced in pA interactions, including k_T broadening and nuclear shadowing. The nuclear dependence is studied over a range of energies, both in fixed target and collider setups.

Introduction

Previously, the heavy quark production cross section was calculated in pp interactions focussing on the scale dependence and fixing the mass and scale as parameters in the total cross section [1]. In this extension to pA interactions, we study the effects of shadowing and p_T broadening on the spectra of heavy quark production.

*This work was supported in part by the Director, Office of Energy Research, Division of Nuclear Physics of the Office of High Energy and Nuclear Physics of the U. S. Department of Energy under Contract Number DE-AC03-76SF00098.

We first briefly discuss the calculation of the total cross section and then go on to discuss the relevant differential distributions.

Total cross section

Recall that at leading order (LO) heavy quarks are produced by gg fusion and $q\overline{q}$ annihilation while at next-to-leading order (NLO), $qg+\overline{q}g$ scattering is also included. At any order, the partonic cross section may be expressed in terms of dimensionless scaling functions $f_{ij}^{(k,l)}$ that depend only on the variable η [2]

$$\hat{\sigma}_{ij}(\hat{s}, m_Q^2, \mu^2) = \frac{\alpha_s(\mu)^2}{m^2} \sum_{k=0}^{\infty} \, (4\pi\alpha_s(\mu))^k \sum_{l=0}^{k} \, f_{ij}^{(k,l)}(\eta) \, \ln^l \left(\frac{\mu^2}{m_Q^2}\right) \, , \tag{1}$$

where $\hat{s}$ is the partonic center of mass, m_Q is the heavy quark mass, μ is the renormalization scale, and $\eta = \hat{s}/4m_Q^2 - 1$. The summation is expanded in powers of α_s with $k = 0$ corresponding to the Born cross section at order $\mathcal{O}(\alpha_s^2)$. The first correction with $k = 1$ corresponds to the NLO cross section at $\mathcal{O}(\alpha_s^3)$. It is only at this order and above that the renormalization scale dependence enters the calculation (aside from the scale dependence of α_s which appears already at leading order) since when $k = 1$ and $l = 1$, the logarithm $\ln(\mu^2/m_Q^2)$ appears. The next-to-next-to-leading order (NNLO) corrections to next-to-leading logarithm have been calculated near threshold [2] but the complete calculation only exists to NLO.

The total partonic cross section can also be written as

$$\hat{\sigma}_{ij}(\hat{s}, m_Q^2, \mu^2) = \int d\hat{t} \, d\hat{u} \, \hat{s}^2 \frac{d\hat{\sigma}_{ij}(\hat{s}, \hat{t}, \hat{u})}{d\hat{t} d\hat{u}} \tag{2}$$

where the double differential partonic cross section at leading order is proportional to the Born cross section,

$$\hat{s}^2 \frac{d\hat{\sigma}_{ij}^{(0)}(\hat{s}, \hat{t}, \hat{u})}{d\hat{t} d\hat{u}} = \delta(\hat{s} - \hat{t} - \hat{u} - 2m_Q^2) \hat{\sigma}_{ij}^B(\hat{s}, \hat{t}, \hat{u}) \, . \tag{3}$$

The NLO and NNLO cross sections in the $q\overline{q}$ channel are also proportional to $\hat{\sigma}_{q\overline{q}}^B$, albeit with more complicated coefficients. In the gg channel, the higher order cross sections are also proportional to the Born cross section to leading logarithm and also for the highest powers of the factorization scale dependent logarithms [2]. The expressions for the Born cross section in both channels may be found in Ref. [2] along with the NLO and NNLO expressions near threshold.

The cross sections may be calculated in either one-particle inclusive kinematics or pair kinematics, depending on whether one or both heavy quarks are detected. Single heavy quark hadroproduction in pp interactions is defined by

$$p(P_1) + p(P_2) \longrightarrow Q(p_1) + X(p_X) \, , \tag{4}$$

where X denotes any hadronic final state containing the heavy antiquark and $Q(p_1)$ is the identified heavy quark. The reaction in Eq. (4) is dominated by the partonic reactions

$$q(k_1) + \overline{q}(k_2) \longrightarrow Q(p_1) + X[\overline{Q}](p_2)\,, \tag{5}$$
$$g(k_1) + g(k_2) \longrightarrow Q(p_1) + X[\overline{Q}](p_2)\,. \tag{6}$$

At LO or if $X[\overline{Q}](p_2) \equiv \overline{Q}(p_2')$, the reaction is at partonic threshold with $\overline{Q}$ momentum p_2'. At threshold the heavy quarks do not have to be produced at rest but are instead produced with equal and opposite momentum, leading to trivial values of the pair transverse momentum ($p_1 + p_2' = 0$) and azimuthal angle ($\phi = \pi$). The Mandelstam invariants on the hadronic level are

$$s = (P_1 + P_2)^2 \quad , \quad t = (P_1 - p_1)^2 \quad , \quad u = (P_2 - p_1)^2\,, \tag{7}$$

with the corresponding partonic invariants

$$\hat{s} = (k_1 + k_2)^2 \quad , \quad \hat{t} = (k_2 - p_1)^2 \quad , \quad \hat{u} = (k_1 - p_1)^2\,. \tag{8}$$

The kinematics of heavy quark pair production is somewhat different with

$$p(P_1) + p(P_2) \longrightarrow Q\overline{Q}(P') + X(P_X)\,. \tag{9}$$

On the parton level, Eqs. (5) and (6) are now

$$q(k_1) + \overline{q}(k_2) \longrightarrow Q\overline{Q}(p') + X(p_X)\,, \tag{10}$$
$$g(k_1) + g(k_2) \longrightarrow Q\overline{Q}(p') + X(p_X)\,. \tag{11}$$

The square of the heavy quark pair mass is $p'^2 = M^2$. In the case when $p_X \neq 0$, more invariants than the three typical Mandelstam invariants can be defined [3]. At partonic threshold, $p_X = 0$, only the three Mandelstam invariants remain with $\hat{s} = M^2$ and

$$\hat{t} - m_Q^2 = -\frac{M^2}{2}(1 - \beta_M \cos\theta)\,, \tag{12}$$
$$\hat{u} - m_Q^2 = -\frac{M^2}{2}(1 + \beta_M \cos\theta)\,, \tag{13}$$

where $\beta_M = \sqrt{1 - 4m_Q^2/M^2}$, and θ is the scattering angle in the parton center of mass frame.

The total hadronic cross section is obtained by convoluting the total partonic cross section with the parton distribution functions from the initial hadrons,

$$\sigma_{pp}(s, m_Q^2) = \sum_{i,j=q,\overline{q},g} \int_{4m_Q^2/s}^{1} \frac{d\tau}{\tau}\, \delta(x_1 x_2 - \tau)\, F_i^p(x_1, \mu^2) F_j^p(x_2, \mu^2)\, \hat{\sigma}_{ij}(\tau, m_Q^2, \mu^2)\,, \tag{14}$$

where the sum is over all massless partons and x_1 and x_2 are the hadron momentum fractions carried by the interacting partons. The parton distribution functions, denoted by F_i^p, are evaluated at the factorization scale, assumed to be equal to the renormalization scale in all our calculations.

In our previous work on pp interactions [1], we obtained our results with two sets of parton distribution functions that had successfully predicted the behavior of the measured parton distributions at low x [4], MRS D$-'$ [5] and GRV HO [6]. Much more data has become available since then which shows that the initial parton densities were too high at low x and fits to the most recent data [7] are now available. Our results are now calculated with the most recent NLO parton distribution functions from the MRS group, MRST HO (mode 1) [8]. This group has also made a leading order set available [9]. We compare the MRS D$-'$, MRST HO, and MRST LO results in Fig. 1 and in Tables 1 and 2, all updated from our earlier work [1]. Table 1 has also been expanded to include the fixed target energies at which we compare the pp and pA calculations.

All the cross sections are calculated at LO and NLO with the same mass and scale parameters obtained from the pp study—$m_c = 1.2$ GeV, $\mu_c = 2m_c$, $m_b = 4.75$ GeV, and $\mu_b = m_b$. The agreement with the total charm cross section data is at least as good with the MRST sets as with the MRS D$-'$ set. In fact, the somewhat larger NLO cross section from MRST HO at fixed target energies tends to agree better with the data than the older set. However, at the pp and AA collider energies shown in Tables 1 and 2, the growth of the cross sections is considerably slower with the new distribution functions than with the MRS D$-'$ set.

The MRST LO results are for comparative purposes only. A LO set is not consistent with a NLO calculation just as a NLO set is inconsistent with a LO calculation. The tabulated results are all calculated using α_s at two loops, regardless of whether the LO or NLO result is given. Since the QCD scale, Λ, is tuned to fit all available data in global analyses of parton distributions, it makes a difference whether a LO or NLO evaluation is consistent. When a full LO calculation of the charm cross section is done with a one loop evaluation of α_s in the global analyses of the parton densities, as with the MRST LO set, the LO cross section in Table 1 increases by $\sim 60\%$. This change is due almost solely to the difference between the one and two loop evaluations of α_s where $\Lambda = 0.204$ when $n_f = 3$ for charm production leading to $\alpha_s^{\rm oneloop} = 0.287$ and $\alpha_s^{\rm twoloops} = 0.220$. In general, the calculations at LO with MRST LO partons agree better with the tabulated LO results for MRST HO partons where the value of Λ is tuned using a two loop evaluation of α_s. Likewise, if the MRS D$-'$ set is used in a LO calculation the LO charm cross section is $\sim 20\%$ smaller because the value of Λ obtained in the NLO global analysis is larger at two loops. These results show that one must use caution when using a LO set with a NLO calculation or a NLO set for a LO calculation.

Differential cross section

While the total cross section predicts the yield of heavy quark production, it cannot provide much useful information on nuclear effects such a p_T-broadening and

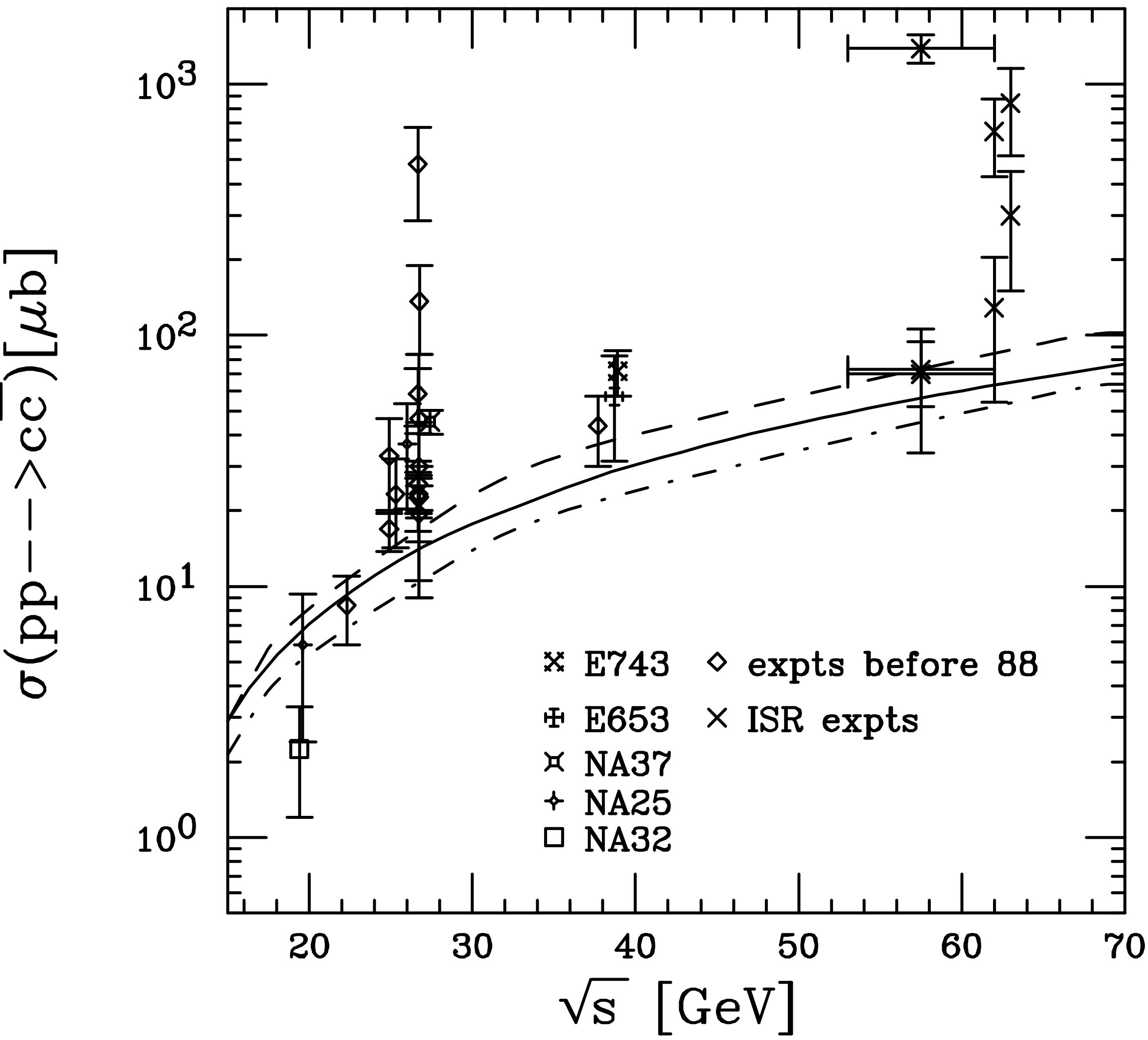

Figure 1: Total charm production cross sections from pp and pA measurements [11, 12, 13, 14, 15] compared to calculations with $m_c = 1.2$ GeV and $\mu = 2m_c$. The parton distributions used are MRS D$-'$ (solid); MRST HO (dashed) and MRST LO (dot-dashed). Updated from Ref. [1].

	MRST LO		MRST HO		MRS D−′	
$\sqrt{s}$(GeV)	$\sigma_{c\overline{c}}^{\rm LO}$ (μb)	$\sigma_{c\overline{c}}^{\rm NLO}$ (μb)	$\sigma_{c\overline{c}}^{\rm LO}$ (μb)	$\sigma_{c\overline{c}}^{\rm NLO}$ (μb)	$\sigma_{c\overline{c}}^{\rm LO}$ (μb)	$\sigma_{c\overline{c}}^{\rm NLO}$ (μb)
17.3	1.40	3.63	1.78	5.29	1.67	4.62
19.4	1.96	4.99	2.59	7.55	2.36	6.38
29.1	5.30	12.84	7.66	21.16	6.42	16.24
38.8	9.63	22.86	14.33	38.32	11.47	28.20
63	23.10	53.86	34.06	87.41	26.88	64.97
200	120.7	279.9	148.5	373.8	139.3	343.7
500	341.4	801.8	353.6	929.9	449.4	1138
5500	2768	6800	1925	5479	7013	17680
14000	5163	12950	2800	8372	16450	41770

Table 1: Total $c\overline{c}$ production cross sections at fixed-target and collider energies.

	MRST LO		MRST HO		MRS D−′	
$\sqrt{s}$(GeV)	$\sigma_{b\overline{b}}^{\rm LO}$ (μb)	$\sigma_{b\overline{b}}^{\rm NLO}$ (μb)	$\sigma_{b\overline{b}}^{\rm LO}$ (μb)	$\sigma_{b\overline{b}}^{\rm NLO}$ (μb)	$\sigma_{b\overline{b}}^{\rm LO}$ (μb)	$\sigma_{b\overline{b}}^{\rm NLO}$ (μb)
63	0.0346	0.0628	0.0383	0.0734	0.0397	0.0746
200	0.690	1.25	0.935	1.80	0.796	1.47
500	3.543	6.752	4.637	9.442	3.847	7.597
5500	76.6	170.6	74.6	193	98.8	224
14000	195.4	457.3	168.5	467.7	296.8	687.5

Table 2: Total $b\overline{b}$ production cross sections at collider energies.

shadowing. It is also independent of the choice of kinematic schemes. Any p_T broadening will not affect the total cross section but will have a strong influence on the p_T distributions. Shadowing may reduce or enhance the nuclear cross section relative to the proton one but the effect may be more apparent in some regions of phase space than others. To obtain more information on nuclear effects, it is thus necessary to turn to distributions.

The double differential hadronic cross sections are written in the factorized form

$$s^2\,\frac{d^2\sigma_{pp}(s,t,u)}{dtdu} = \sum_{i,j=q,\overline{q},g}\int_{x_1^-}^1 \frac{dx_1}{x_1}\int_{x_2^-}^1 \frac{dx_2}{x_2} f_i^p(x_1,\mu^2) f_j^p(x_2,\mu^2)\mathcal{J}_K(\hat{s},\hat{t},\hat{u})\hat{s}^2\frac{d^2\sigma_{ij}(\hat{s},\hat{t},\hat{u})}{d\hat{t}d\hat{u}}\ , \quad (15)$$

where f_i^p is the parton density, $f_i^p(x,\mu^2) = F_i^p(x,\mu^2)/x$, and $\mathcal{J}_K$ is a kinematics-dependent Jacobian. These results are difficult to calculate analytically and expressions only exist for $\hat{s}^2 d^2\sigma_{ij}(\hat{s},\hat{t},\hat{u})/d\hat{t}d\hat{u}$, see *e.g.* [2]. However, there is a scheme to obtain the results numerically that has been successfully used to model heavy quark production over a wide range of energies—a program by Nason, Mangano, and Ridolfi [3] that is generally available. In our first paper [1], we neglected any fragmentation or intrinsic transverse momentum of the initial partons because the inclusive D meson p_T distributions agreed with the bare charm quark distributions, showing no need for such effects. However, as pointed out in Ref. [10], the pair distributions, particularly the pair p_T and the azimuthal angle distributions at fixed target energies are broader than can be accounted for by the bare quark distributions. They were able to reproduce the general behavior of the data by including a Peterson-type fragmentation function [16] along with an intrinsic k_T of the initial partons. Indeed, the combination of fragmentation with an intrinsic average k_T^2 of 1 GeV^2 leads to single D meson p_T distributions in good agreement with the bare charm distribution. These effects can be included by modifying Eq. (15) to include the additional integrals

$$\int dz_3 dz_4 d^2k_{T1} d^2k_{T2} \frac{D_{H/Q}(z_3,\mu^2)}{z_3} \frac{D_{\overline{H}/\overline{Q}}(z_4,\mu^2)}{z_4} g_p(k_{T1}) g_p(k_{T2}) \ . \tag{16}$$

The fragmentation functions $D_{H/Q}(z)$ describe the hadronization of the heavy quark Q into hadron H. The final-state hadron H carries a fraction z of the heavy quark momentum and is assumed to be collinear with the parent heavy quark. The Peterson fragmentation function [16], fit to D production data in e^+e^- collisions,

$$D_{H/Q}(z) = \frac{N}{z(1-1/z-\epsilon_Q/(1-z))^2} \ , \tag{17}$$

is used in the code. The parameter ϵ_Q is 0.06 for charm and 0.006 for bottom [17]. The normalization N is defined by $\sum_H \int D_{H/Q}(z)dz = 1$.

The Peterson function results in a nearly 30% decrease in the average charm quark momentum during hadronization. This decrease must be compensated for in inclusive production because the decreased momentum of the D meson would no longer agree with the single D p_T distributions. The intrinsic k_T of the initial partons is such a mechanism which has been used successfully in the p_T distributions of other processes such as Drell-Yan [19] and hard photon production [20]. Some of the low p_T Drell-Yan data has subsequently been described by resummation to all orders but the inclusion of higher orders has not eliminated the need for this intrinsic k_T. It was found that by assuming $\langle k_T^2 \rangle = 1$ GeV^2 in pp and πp interactions produces agreement with the inclusive data on the level of that found with the bare quarks alone but does a better job of reconciling the exclusive $D\overline{D}$ distributions with the calculations [10].

The implementation of intrinsic k_T in the MNR code is not the same as in other processes due to the nature of their calculation. The cancellation of divergences is handled numerically in the code. Since adding additional numerical integrations would slow this process, the k_T kick is added in the final, rather than the initial state. In Eq. (16), the Gaussian function $g_p(k_T)$,

$$g_p(k_T) = \frac{1}{\pi \langle k_T^2 \rangle_p} \exp(-k_T^2/\langle k_T^2 \rangle_p) \tag{18}$$

with $\langle k_T^2 \rangle_p = 1$ GeV^2 [10], multiplies the parton distribution functions, assuming the x and k_T dependencies completely factorize. If this is true, it does not matter whether the k_T dependence appears in the initial or final state modulo the caveat described below. In the code, the $Q\overline{Q}$ system is boosted to rested from its longitudinal center of mass frame. Transverse momenta of the incoming partons, $\vec{k}_{T1}$ and $\vec{k}_{T2}$, are chosen at random with k_{T1}^2 and k_{T2}^2 distributed according to Eq. (18). A second transverse boost out of the pair rest frame changes the initial transverse momentum of the $Q\overline{Q}$

pair, $\vec{p}_T'$ in Eqs. (10) and (11), to $\vec{p}_T' + \vec{k}_{T1} + \vec{k}_{T2}$. The initial k_T of the partons could have alternatively been given to the entire final-state system, as is essentially done if applied in the initial state, instead of to the $Q\overline{Q}$ pair. There is no difference if the calculation is to LO only but at NLO an additional light parton also appears in the final state. In Ref. [18], they claim that the difference in the two method is rather small if $k_T^2 \leq 2$ GeV^2. The effect of the intrinsic k_T decreases as the center of mass energy increases.

k_T broadening

The average intrinsic k_T is expected to increase in pA interactions. This broadening is observed in Drell-Yan [21], J/ψ [22], and Υ [21] production and has been used to explain high p_T pion production in nuclear interactions [24]. Since k_T broadening has not been explicitly measured in charm production, we follow the formulation of Ref. [24], similar to Ref. [23] for J/ψ and Drell-Yan production where the k_T broadening arises from multiple scattering of the projectile partons in the target,

$$\langle k_T^2 \rangle_A = \langle k_T^2 \rangle_p + (\langle \nu \rangle - 1)\Delta^2(\mu) \ . \tag{19}$$

We use the number of collisions, averaged over impact parameter,

$$\langle \nu \rangle = \sigma_{NN} \frac{\int d^2b T_A^2(b)}{\int d^2b T_A(b)} = \frac{3}{2} \sigma_{NN} \rho_0 R_A \ , \tag{20}$$

where $T_A(b)$ is the nuclear profile function, to calculate the broadening and vary this average by a factor of two to similate different centralities and uncertainties. In $\langle \nu \rangle$, σ_{NN} is the inelastic nucleon-nucleon scattering cross section, ρ_0 is the central nuclear density, and R_A is the nuclear radius. Our calculations are done with $A = 200$, $R_A = 1.2A^{1/3}$, and $\rho_0 = 0.16/\text{fm}^3$.

The strength of the nuclear broadening, Δ^2, depends on μ, the scale of the interaction [24]

$$\Delta^2(\mu) = 0.225 \frac{\ln^2(\mu/\text{GeV})}{1 + \ln(\mu/\text{GeV})} \text{GeV}^2 \tag{21}$$

The expression for Δ^2 is scale dependent so that Δ^2 is larger for $b\overline{b}$ production than $c\overline{c}$ production. This empirically reflects the larger k_T broadening of the Υ [21] relative to the J/ψ [22]. We use $\langle k_T^2 \rangle_A = 1.35 \pm 0.17$ GeV^2 for charm and $\langle k_T^2 \rangle_A = 2.57 \pm 0.79$ GeV^2, both evaluated at $\mu = 2m_Q$ to study the effect of k_T broadening on charm and bottom production.

The effects of k_T broadening alone on several pair and single inclusive quantities are shown for a fixed target beam energy of 158 GeV in Figs. 2 and 3. The pair quantities in Fig. 2 is rather striking. The bare charm pair distributions alone are compared to results with $\langle k_T^2 \rangle = 1 - 1.7$ GeV^2. The difference in the pair p_T and ϕ distributions is striking. The broadening of the pair p_T distribution is due entirely to

k_T broadening since fragmentation effects would act to steepen the solid curve. The broadening is still important at large pair p_T, causing more than an order of magnitude difference in the cross section between $\langle k_T^2 \rangle = 1$ GeV^2 and 1.7 GeV^2 at $p_T = 4$ GeV. Likewise, introducing intrinsic k_T changes the ϕ distribution from sharply peaked at $\phi = \pi$ for the bare charm quarks to nearly flat when $\langle k_T^2 \rangle = 1$ GeV^2 to a peak at $\phi = 0$ when $\langle k_T^2 \rangle = 1.7$ GeV^2. On the contrary, the pair rapidity shows no effect of k_T broadening.

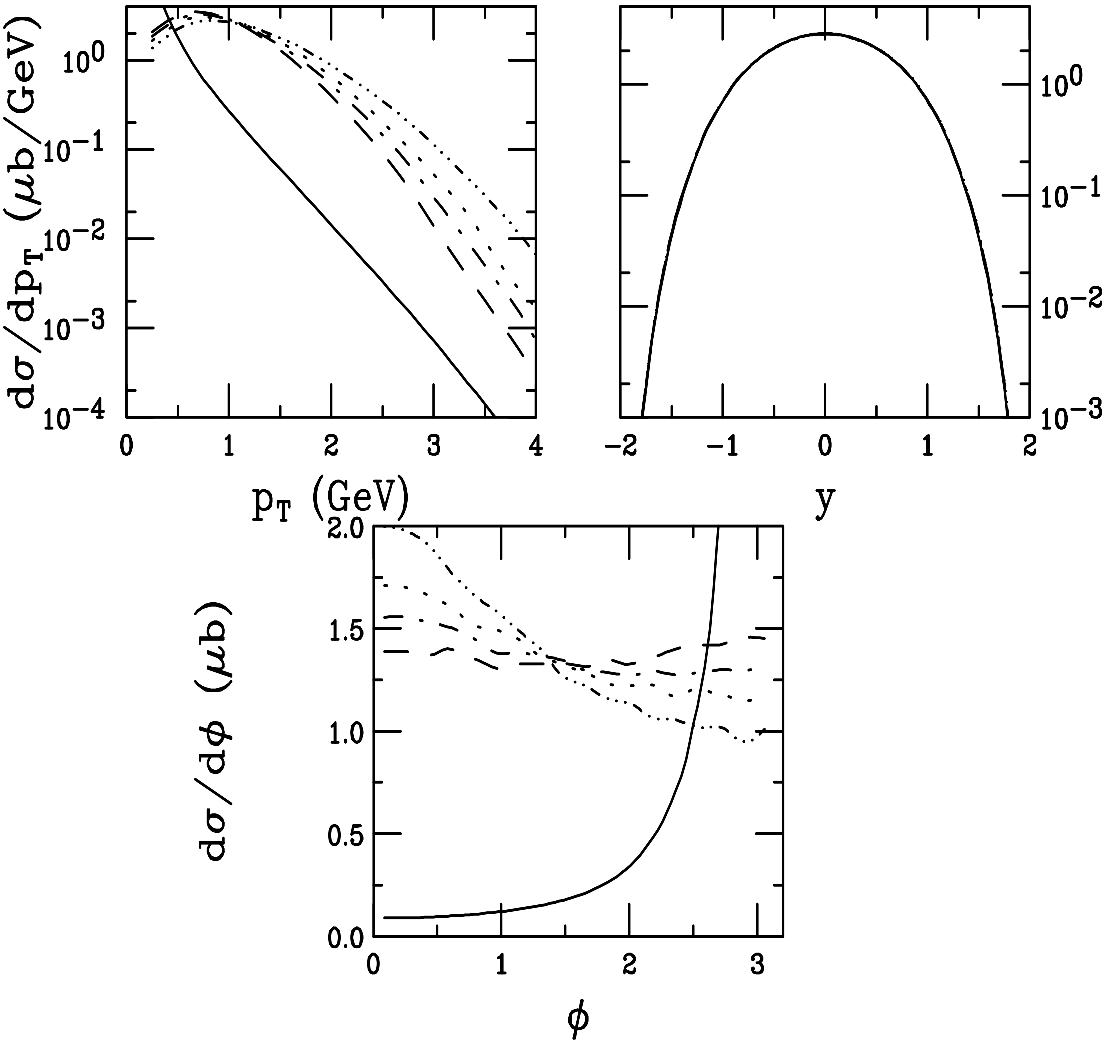

Figure 2: Effects of k_T broadening alone on exclusive NLO $c\bar{c}$ pair production in pA interactions at 158 GeV as a function of p_T, y, and ϕ. The per nucleon cross section is given. The curves are the bare quark distributions alone ($\langle k_T^2 \rangle_A = 0$ and no fragmentation) (solid) and, including fragmentation, $\langle k_T^2 \rangle = 1$ (dashed), 1.175 (dot-dashed), 1.35 (dotted) and 1.7 (dot-dot-dot-dashed) GeV^2.

The broadening effect is not as strong for the single charm distributions shown in Fig. 3. Note that all the distributions, including the charm rapidity distribution, are affected by broadening and fragmentation. The charm p_T distributions for the bare quark and including fragmentation with $\langle k_T^2 \rangle = 1$ GeV^2 are almost identical, in accord with the observation that no intrinsic k_T was needed to describe the D meson p_T distributions. The difference between the bare quark and $\langle k_T^2 \rangle = 1.7$ GeV^2 is less than a factor of five for $p_T = 3.5$ GeV. Fragmentation is the most important effect on the x_F and rapidity distributions since there is little change in the distributions as $\langle k_T^2 \rangle$ is increased. Any type of fragmentation, even that of a delta function, will cause the rapidity and x_F distributions to be modified. This is because fragmentation enhances these distributions in the central region [25]. If $D_{H/Q}(z)$ is a delta function, the momentum does not change, $p_Q = p_H$, but $E_Q^2 = E_H^2 - m_H^2 + m_Q^2$, resulting in a rapidity shift [25] with

$$dn \propto dy_Q = \frac{dp_{zQ}}{E_Q} = \frac{dp_{zH}}{E_Q} = \frac{m_{T,H} \cosh y_H dy_H}{\sqrt{m_{T,H}^2 \cosh^2 y_H - m_H^2 + m_Q^2}} \approx \frac{\cosh y_H dy_H}{\sqrt{\cosh^2 y_H - \alpha^2}} \quad (22)$$

where

$$\alpha^2 = \frac{m_H^2 - m_Q^2}{m_{T,H}^2} \ . \quad (23)$$

For $m_c = 1.2$ GeV, $m_D = 1.87$ GeV and $m_{T,D} \approx \sqrt{2} m_D$, $\alpha^2 = 0.25$, enhancing the D distribution at $y = 0$ by $\approx 15\%$. When $m_b = 4.75$ GeV, $m_B = 5.27$ GeV and $m_{T,B} = \sqrt{2} m_B$, $\alpha^2 = 0.09$, enhancing the B distribution by $\approx 5\%$. The range of the enhancement is $|y_H| < 2.5$, independent of energy. If the Peterson function is used instead, α^2 increases,

$$\alpha^2 = \frac{m_H^2 - z^2 m_Q^2}{m_{T,H}^2} \ , \quad (24)$$

increasing the D enhancement at $y_H = 0$ to $\approx 30\%$ for $\langle z \rangle \approx 0.7$ and the B enhancement to $\approx 15\%$ for $\langle z \rangle \approx 0.85$. These $\langle z \rangle$ values are typical for the Peterson function with ϵ values given above. The x_F distribution is also affected because $x_F = 2 m_T \sinh y / \sqrt{s}$.

Nuclear shadowing

Experiments [26] have shown that the proton and neutron structure functions are modified by a nuclear environment. For momentum fractions $x < 0.1$ and $0.3 < x < 0.7$, a depletion is observed in the nuclear parton distributions. The low x, or shadowing, region and the larger x, or EMC region, is bridged by an enhancement known as antishadowing for $0.1 < x < 0.3$. For simplicity, the entire characteristic modification as a function of x has been referred to as shadowing.

Shadowing is an area of intense study with numerous models available in the literature [26]. However, none of the models can satisfactorily explain the behavior of the nuclear parton distributions over the entire x and μ^2 range. Therefore, we choose to use parameterizations of shadowing based on nuclear DIS data. As in DIS

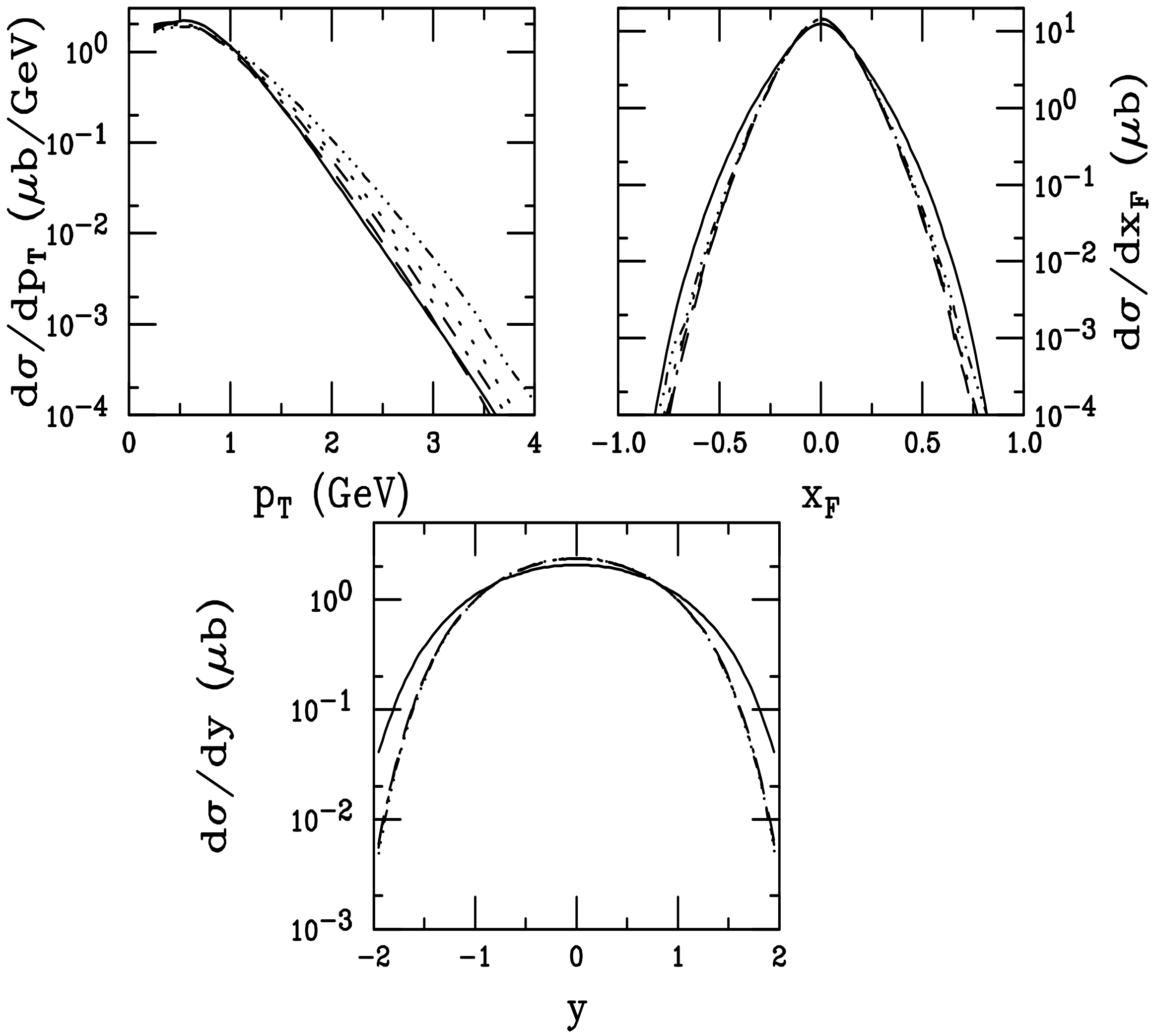

Figure 3: Effects of k_T broadening alone on inclusive NLO c quark production in pA interactions at 158 GeV as a function of p_T, x_F, and y. The per nucleon cross section is given. The curves are the bare quark distributions alone ($\langle k_T^2 \rangle_A = 0$ and no fragmentation) (solid) and, including fragmentation, $\langle k_T^2 \rangle = 1$ (dashed), 1.175 (dot-dashed), 1.35 (dotted) and 1.7 (dot-dot-dot-dashed) GeV^2.

with protons, the nuclear gluon distribution is not directly measured and can only be inferred from conservation rules. We use the recent EKS98 parameterization based on the GRV LO [6] parton densities in the proton. Each parton type is evolved separately above $\mu_0 = 1.5$ GeV [28, 29]. The initial gluon distribution in shows significant antishadowing for $0.1 < x < 0.3$ while the sea quark distributions are shadowed. Figure 4 compares shows the shadowing ratios at $\mu = \mu_0$ and $\mu = 10$ GeV. The valence ratio changes little with scale but the evolution of the gluon and sea ratios with scale is more significant. The gluon ratio changes somewhat more rapidity with scale that the sea ratio but the difference is not large. Less shadowing is seen in the antishadowing region at larger scales for the sea quark ratio while the gluon ratio decreases with scale in the same region.

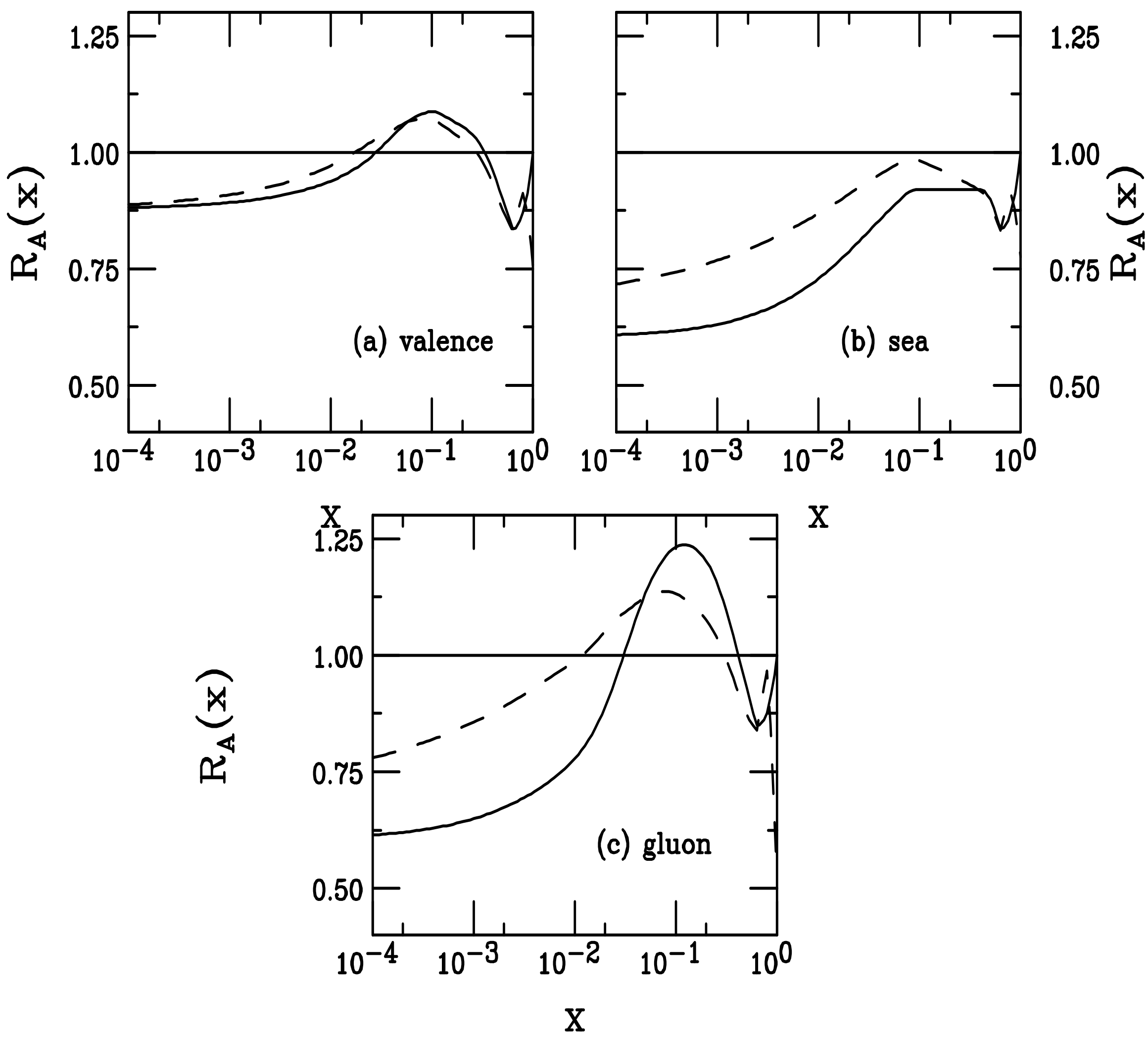

Figure 4: The shadowing parameterizations for $A = 200$ for (a) u_V valence quarks, (b) $\overline{u}$ sea quarks, and (c) gluons. The solid curves show the ratios at $\mu = \mu_0$ while the dashed curves are at $\mu = 10$ GeV.

Shadowing should depend on the spatial location of the parton in the nucleus.

Unfortunately, there is little data on this topic. One relevant experiment, Fermilab E745, studied the spatial distribution of nuclear parton densities with νN interactions in emulsion. The presence of one or more dark tracks from slow protons is used to infer a more central interaction[27]. For events with no dark tracks, no shadowing is observed while for events with dark tracks, shadowing is enhanced over other experimental measurements insensitive to the spatial location.

The spatial dependence of nuclear shadowing has been studied in charm and bottom production [30, 31]. While the effect can be important in peripheral collisions since nucleons near the nuclear surface are expected to behave as free particles, in central collisions where modifications are larger than average, this increase is $\sim 1\%$ over the average, negligible for our purposes.

Rates

To calculate the rate of charm and bottom production in these interactions as a function of impact parameter, the per nucleon $Q\overline{Q}$ cross sections for pA interactions given in this paper, should be multiplied by the nuclear profile function, $T_A(b) = \int dz \rho_A(b,z)$,

$$N_A^{Q\overline{Q}}(b) = \sigma_{pA}^{Q\overline{Q}} T_A(b) \ . \tag{25}$$

Thus, over all impact parameters, the pA cross section should scale as A times the pp cross section without any nuclear effects. Since the only nuclear effect that can change the total cross section is shadowing, total charm and bottom production should have a nearly linear A dependence except at very high energies where the shadowing effects will be larger.

We note that in the case of pA interactions, the impact parameter dependence of charm and bottom production is the same as that of the geometric cross section. This similarity arises because the average number of collisions and the average number of participants is the same in pA interactions. In nucleus-nucleus collisions, hard production is biased toward central collisions, see Ref. [32] for more details.

Results

We will show inclusive charm and bottom and exclusive $c\overline{c}$ and $b\overline{b}$ production at several different energies. First we show fixed target charm production at 158, 450, and 800 GeV. These energies are chosen because Pb+Pb interactions are studied at the CERN SPS at 158 GeV/nucleon and it would be useful to examine charm production in pp and pPb interactions at the same energy. However, since this would require a secondary beam, we also show the results at the SPS primary proton beam energy of 450 GeV. The Fermilab fixed target program has an 800 GeV beam which could also be used for studies of the charm A dependence. Indeed, a great many experiments have studied charm production, both at CERN and at Fermilab but unfortunately the statistics for proton beams have generally been poor and the results have not been used to determine the A dependence. Better statistics are available for π beams but the data is typically averaged over all targets to enhance statistics rather than to study the A dependence. Since the RHIC and LHC heavy ion programs will include pA studies, we also show results at the complementary ion-ion energy, $\sqrt{s} = 200$ GeV/nucleon and 5.5 TeV/nucleon, respectively.

All the pp calculations are shown with $\langle k_T^2 \rangle = 1$ GeV^2 and all the pA calculations are presented with $\langle k_T^2 \rangle = 1.35$ GeV^2 for charm and 2.57 GeV^2 for bottom. The pA calculations are modified by spatially homogeneous shadowing with the recent parameterization by Eskola and collaborators [28, 29] at $A = 200$.

We first show that the theoretical K factor, $K_{\rm th}$, the ratio of the NLO to LO cross sections, both calculated with MRST HO in the MNR code is constant in pp and pA interactions at 158 GeV in Fig. 5. There is some variation near the edges of phase space where the statistics become poor. However, we have checked that neither shadowing nor k_T broadening lead to significant changes in $K_{\rm th}$. The same K factors have also been calculated at collider energies have been shown in Ref. [33] for the MRS D$-'$ distributions and are also constant. The exact value of $K_{\rm th}$ depends on the set of parton distributions chosen and the interaction energy.

The exclusive and inclusive cross sections are shown for all energies considered in Figs. 6-19. The exclusive results are given for the pair p_T, rapidity, and ϕ distributions while the inclusive results are given as a function of quark p_T, x_F, and rapidity. Note that at collider energies, we do not show the x_F results since they are very narrow at high energies and the rapidity distributions contain more useful information. The pair p_T and ϕ distributions and the quark p_T distribution all show the effect of k_T broadening in pA over pp interactions. The broadening is most apparent at fixed target energies and at low p_T for the collider energies. The effect is always stronger on the pair quantities. On the other hand, information on nuclear shadowing is more likely to be obtained from the rapidity distributions. The best place to study shadowing effects is in the pair rapidity distribution since Fig. 2 showed that neither k_T broadening nor fragmentation affected the pair rapidity. While the quark rapidity distribution in Fig. 3 did show a difference between the bare quark rapidity distribution and the distributions with k_T broadening included, the change is due to fragmentation rather than the k_T effect. Since shadowing is not symmetric around $y = 0$, we present results over all rapidity and x_F. Tables of the pair and single quark p_T and pair and single quark rapidity for both the pp and pA results are given.

As the center of mass energy is increased, the k_T broadening effect on the $c\overline{c}$ pair p_T and ϕ distributions is seen to diminish in Figs. 6, 8, 10, 12, and 16. At the same time, the pA pair rapidity distributions exhibit a depletion at forward x_F relative to the pp distribution. This effects, most visible on the linear scale of Fig. 16, is due to shadowing and is biased toward forward rapidities where the smallest target x values are probed, $x_2 \sim 3 \times 10^{-6}$ for pairs with $p_T \sim 0$ and $y = 5$. The $b\overline{b}$ pair results in Figs. 14 and 18 exhibit the same basic trends. Note however that the $b\overline{b}$ pairs tend to have much larger p_T than the charm quarks.

The pair p_T is generally higher than for single quarks at any given energy. At NLO, large p_T $Q\overline{Q}$ pairs come from *e.g.* $gg \to gg$ jets where one final state gluon

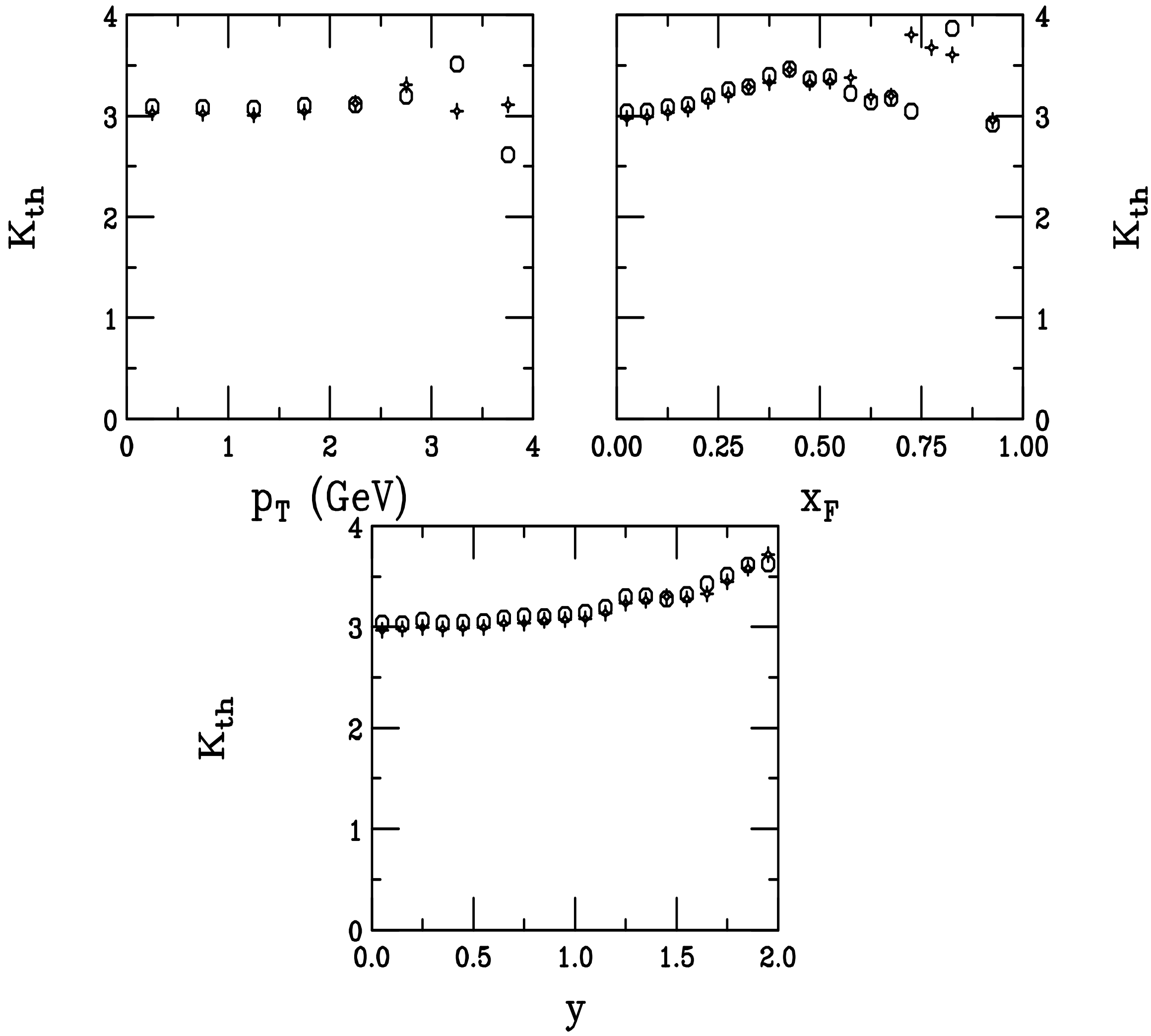

Figure 5: Ratio of NLO to LO c quark production in pp and pA interactions at 158 GeV as a function of p_T, x_F, and y. The crosses are the pp results while the circles are the pA results.

splits into $Q\overline{Q}$, $g \to Q\overline{Q}$. In this way, the pair gets the entire p_T of the gluon while the single quark gets only a fraction of the gluon p_T. Conversely the single quark rapidity is generally greater than that of the pair. That is because $y_{Q\overline{Q}} = 1/2 \ln((E_Q + E_{\overline{Q}} + p_{zQ} + p_{z\overline{Q}})/(E_Q + E_{\overline{Q}} - p_{zQ} - p_{z\overline{Q}}))$ so that if p_{zQ} is large and positive, it may be balanced by a large negative $p_{z\overline{Q}}$. The single quark nuclear effects show the same trends as those of the pair. Note that the single quark p_T distributions are all for $x_F > 0$ only.

Fig. 20 shows the effect of shadowing alone on the pA/pp ratios of the bare charm quark distributions at 158 GeV. Without k_T broadening, the ratio decreases with p_T since $x_2 \sim 0.5$ at $y = 0$, well into the EMC region where the shadowing ratio decreases with x. The effect at low p_T can be observed in the x_F and y ratios where the ratios tend to be greater than unity since x_2 is in the antishadowing region, $x_2 \sim 0.14$ at $y = 0$ and ~ 0.05 at $y = 1$, still in the antishadowing region for gluons with low μ^2. The LO and NLO ratios, both calculated with MRST HO, are quite similar so that the order of the calculation is not strongly influenced by shadowing.

Since the differences between the distributions are not always obvious in Figs. 6-19, we have also calculated the pA to pp ratios, shown in Figs. 21-34. The pair and single quark p_T ratios reflect the effects of the k_T broadening, as do the x_F distributions for $|x_F| > 0.5$. The k_T broadening follows the energy dependent trend predicted in Ref. [34]. The pA/pp ratio increases with p_T at low energies and, as the energy increases, begins to turn over at pair $p_T \sim 3.5 - 4$ GeV for charm, decreasing to unity at large pair p_T. This turnover is at ~ 5 GeV for bottom. As the energy increases, shadowing becomes more important at low p_T, decreasing the ratio below unity in this region. The magnitude of this decrease is a good indication of the strength of gluon shadowing, particularly for the pair. While the single quark ratios follow the trends of the pair ratios at low p_T, the statistics at high p_T leads to large fluctuations. We have checked that taking the single p_T ratio for all x_F rather than $x_F > 0$, as is shown in the figures, neither strongly influences the final results nor significantly improves the fluctuations. These fluctuations are particularly strong in $c\overline{c}$ production at $\sqrt{s} = 5.5$ TeV where both the pair and single charm p_T distributions decrease 4-5 orders of magnitude over the p_T interval shown. The ϕ ratios decrease as ϕ goes from 0 to π because the larger k_T kick in pA flattens this distribution relative to pp so that $pA/pp > 1$ at $\phi \sim 0$ and less than unity at $\phi \sim \pi$, compare Fig. 6 to Fig. 21. The general trend is similar for all energies because variables more sensitive to shadowing are integrated over.

On the other hand, the rapidity ratios follow the gluon ratios shown in Fig. 4. The peak at $x \to 1$ from Fermi motion appears at large negative rapidity, followed by the dip in the EMC region, a broad peak tracing out the antishadowing region, and finally decreasing again as the shadowing region is reached at large, positive rapidity. The shape is inverted from that in Fig. 4 because large x corresponds to large negative rapidity and low x to large positive rapidity. The strength of the shadowing effect increases as energy increases while the antishadowing peak, broad at 158 GeV, narrows with increasing energy. At collider energies, the full rapidity distribution is not shown in the plots so the x distribution of Fig. 4 is somewhat truncated. Both the single and pair rapidity distributions follow the shape of the gluon shadowing ratio, suggesting that either can help elucidate gluon modifications in the nucleus without significant distortion from k_T broadening which affects the x_F ratios.

Conclusions

We have studied the effects of k_T broadening and nuclear shadowing on charm and bottom production over a wide range of energy. We have found that the $Q\overline{Q}$ p_T, the single quark p_T and the pair ϕ distribution are most sensitive to the effects of k_T broadening while the pair and single quark rapidities are sensitive to shadowing. There is significantly less distortion of the nuclear effects in the pair distributions which are the most difficult to measure. The same results may be obtained through measurements of the single heavy quarks event though the definitions of x and k_T are smeared relative to those of the pair.

References

[1] P.L. McGaughey *et. al.*, Int. J. Mod. Phys. **A10** (1995) 2999.

[2] N. Kidonakis, E. Laenen, S. Moch, and R. Vogt, in preparation.

[3] M.L. Mangano, P. Nason, and G. Ridolfi, Nucl. Phys. **B373** (1992) 295.

[4] M. Derrick *et al.* (ZEUS Collab.), Phys. Lett. **B316** (1993) 515.

[5] A.D. Martin, W.J. Stirling and R.G. Roberts, Phys. Lett. **306B**, 145 (1993).

[6] M. Glück, E. Reya, and A. Vogt, Z. Phys. **C53** 127, (1992).

[7] C. Adloff *et al.* (H1 Collab.), Nucl. Phys. **B497** 3, (1997); J. Breitweg *et al.* (ZEUS Collab.), Eur. Phys. J. **C7** 609, (1999).

[8] A.D. Martin, R.G. Roberts, and W.J. Stirling, and R.S. Thorne, Eur. Phys. J. **C4** (1998) 463.

[9] A.D. Martin, R.G. Roberts, and W.J. Stirling, and R.S. Thorne, Phys. Lett. **B443** (1998) 301.

[10] S. Frixione, M.L. Mangano, P. Nason, and G. Ridolfi, Nucl. Phys. **B431** (1994) 453.

[11] S.P.K. Tavernier, Rep. Prog. Phys. **50** (1987) 1439. This review contains references to all data prior to 1988, including the ISR measurements.

[12] R. Ammar *et al.* (LEBC-MPS Collab.), Phys. Rev. Lett. **61** (1988) 2185.

[13] K. Kodama *et al.* (E653 Collab.), Phys. Lett. **B263** (1991) 573.

[14] M. Aguilar-Benitez *et al.* (LEBC-EHS Collab.), Z. Phys. **C40** (1988) 321.

[15] S. Barlag *et al.* (ACCMOR Collab.), Z. Phys. **C39** (1988) 451.

[16] C. Peterson, D. Schlatter, I. Schmitt, and P. Zerwas, Phys. Rev. **D27** (1983) 105.

[17] J. Chirn, in proceedings of the 'International Symposium on the Production and Decay of Heavy Flavors', Stanford, CA, E. Bloom and A. Fridman editors, (1987) p. 131.

[18] S. Frixione, M.L. Mangano, P. Nason, and G. Ridolfi, in 'Heavy flavours II', A.J. Buras and M. Lindner editors, (World Scientific, 1997) p. 609, hep-ph/9702287.

[19] R.D. Field, *Applications of Perturbative QCD*, Frontiers in Physics Lectures, Vol. 77 (Addison-Wesley, Reading, MA, 1989).

[20] J.F. Owens, Rev. Mod. Phys. **59** (1987) 465.

[21] D.M. Alde *et al.* (E772 Collab.), Phys. Rev. Lett. **66** (1991) 2285.

[22] J. Badier *et al.* (NA3 Collab.), Z. Phys. **C20** (1983) 101.

[23] S. Gavin and M. Gyulassy, Phys. Lett. **B214** (1988) 241; J. Hüfner, Y. Kurihara, and H.J. Pirner, Phys. Lett. **B215** (1988) 218; J.-P. Blaizot and J.-Y. Ollitrault, Phys. Lett. **B217** (1989) 392.

[24] X.-N. Wang, Phys. Rev. Lett. **81** (1998) 2655.

[25] Z. Lin and R. Vogt, Nucl. Phys. **B544** (1999) 339.

[26] J.J. Aubert *et al.* (EM Collab.), Nucl. Phys. **B293** 740, (1987); M. Arneodo, Phys. Rep. **240** 301, (1994).

[27] T. Kitagaki *et al.* (E745 Collab.), Phys. Lett. **214** (1988) 281.

[28] K.J. Eskola, V.J. Kolhinen and P.V. Ruuskanen, Nucl. Phys. **B535** 351, (1998).

[29] K.J. Eskola, V.J. Kolhinen and C.A. Salgado, Eur. Phys. J. **C9** (1999) 61.

[30] V. Emel'yanov, A. Khodinov, S.R. Klein and R. Vogt, Phys. Rev. **C56**, 2726 (1997).

[31] V. Emel'yanov, A. Khodinov, S.R. Klein and R. Vogt, Phys. Rev. Lett. **81**, 1801 (1998).

[32] R. Vogt, Heavy Ion Phys. **9** (1999) 339.

[33] R. Vogt, Z. Phys. **C71** (1996) 475.

[34] X.-N. Wang, nucl-th/9812021.

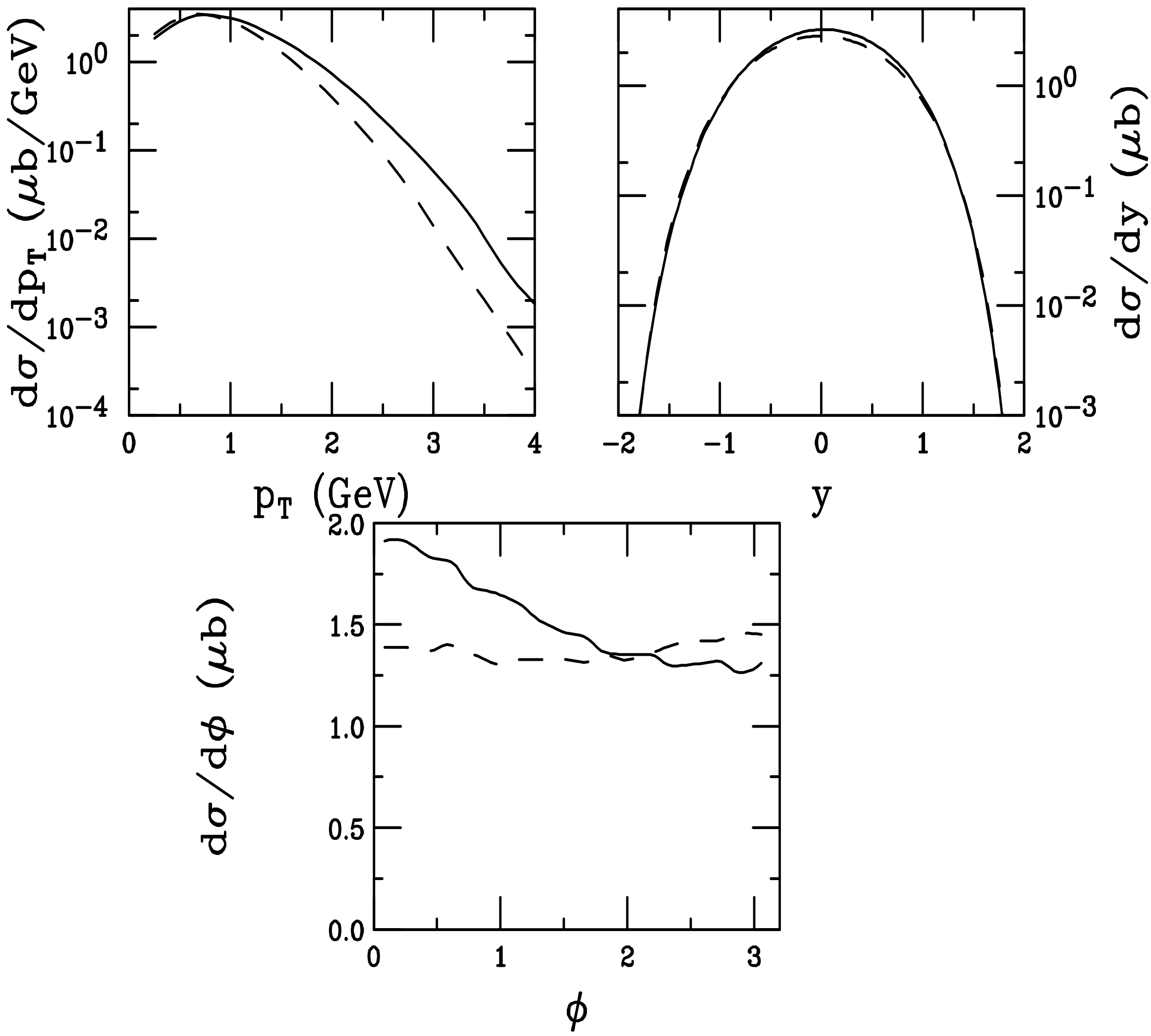

Figure 6: Exclusive NLO $c\overline{c}$ pair production in pp and pA interactions at 158 GeV as a function of p_T, y, and ϕ. The per nucleon cross section is given for pA interactions. The dashed curves are the pp results while the solid curves are the pA results.

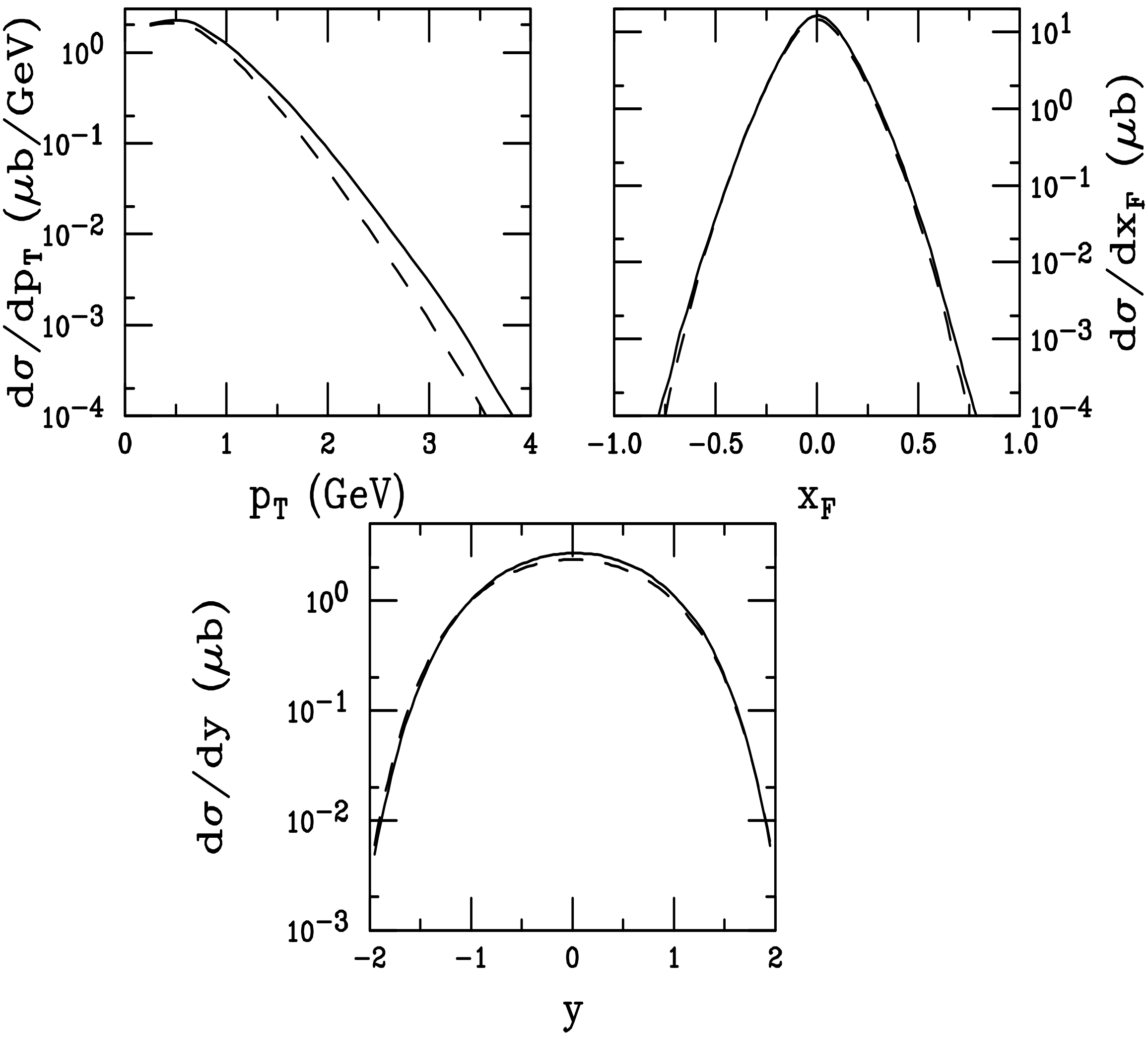

Figure 7: Inclusive NLO c quark production in pp and pA interactions at 158 GeV as a function of p_T, x_F, and y. The p_T distributions are integrated over $x_F > 0$ only. The per nucleon cross section is given for pA interactions. The dashed curves are the pp results while the solid curves are the pA results.

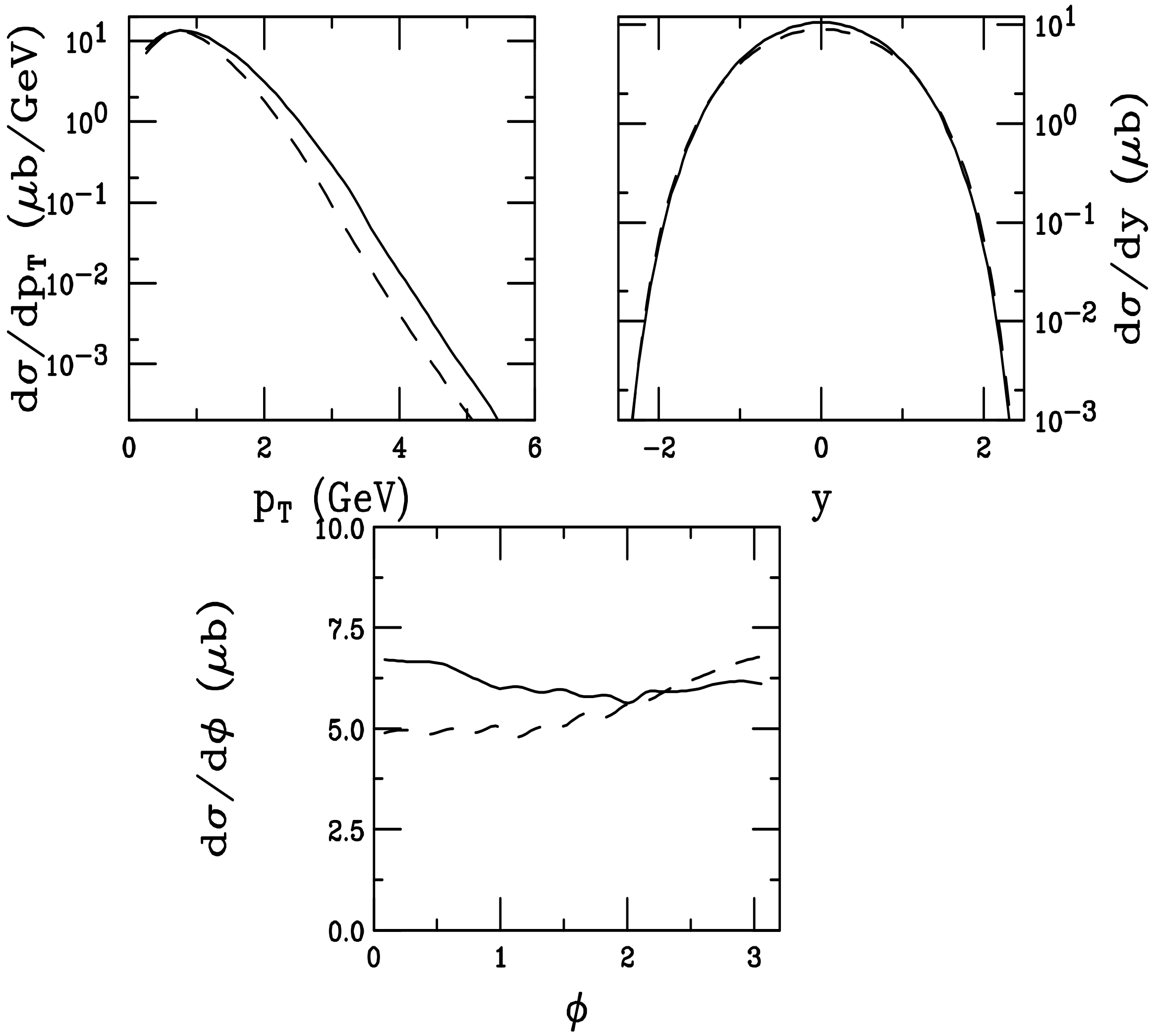

Figure 8: Exclusive NLO $c\bar{c}$ pair production in pp and pA interactions at 450 GeV as a function of p_T, y, and ϕ. The per nucleon cross section is given for pA interactions. The dashed curves are the pp results while the solid curves are the pA results.

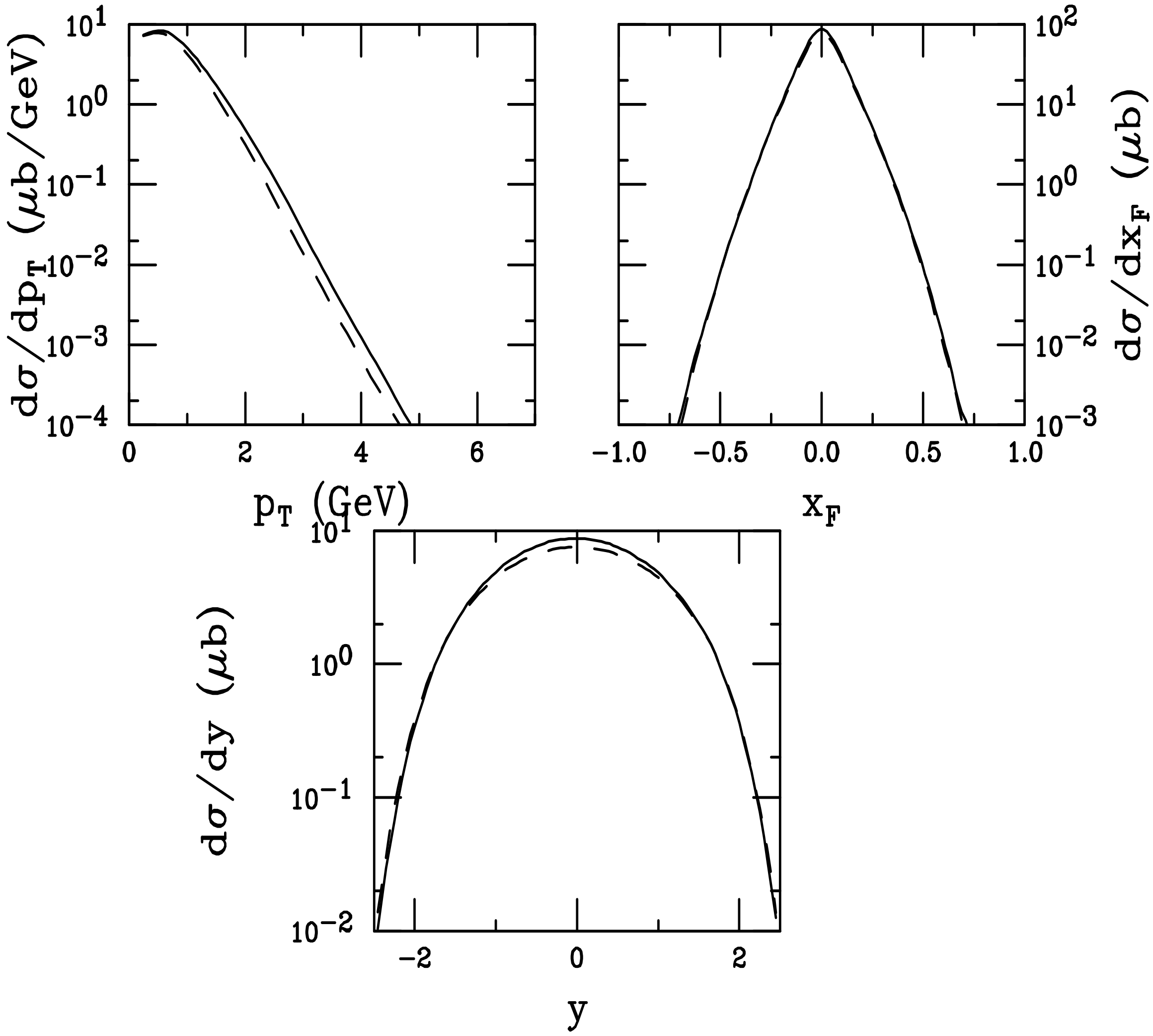

Figure 9: Inclusive NLO c quark production in pp and pA interactions at 450 GeV as a function of p_T, x_F, and y. The p_T distributions are integrated over $x_F > 0$ only. The per nucleon cross section is given for pA interactions. The dashed curves are the pp results while the solid curves are the pA results.

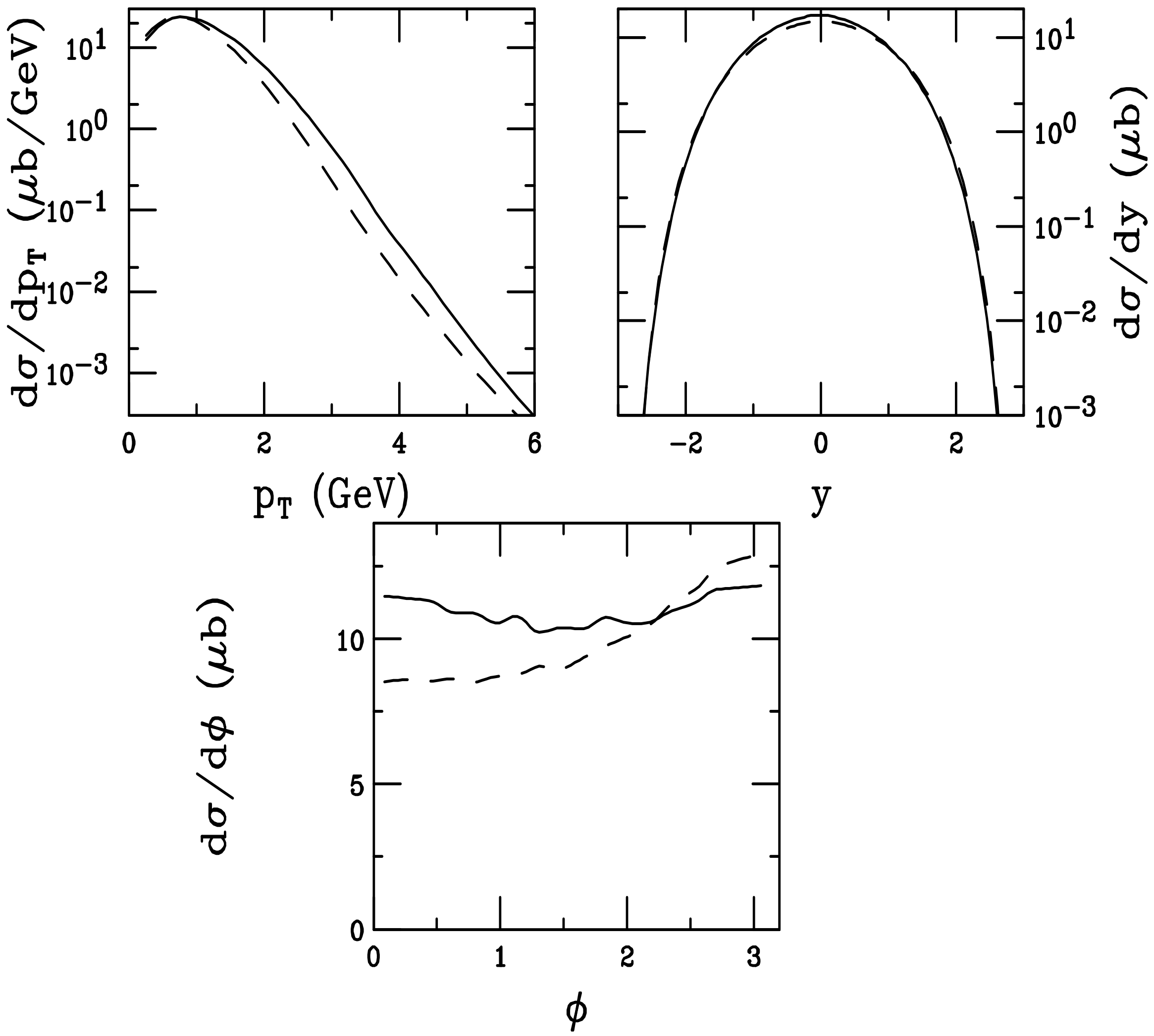

Figure 10: Exclusive NLO $c\overline{c}$ pair production in pp and pA interactions at 800 GeV as a function of p_T, y, and ϕ. The per nucleon cross section is given for pA interactions. The dashed curves are the pp results while the solid curves are the pA results.

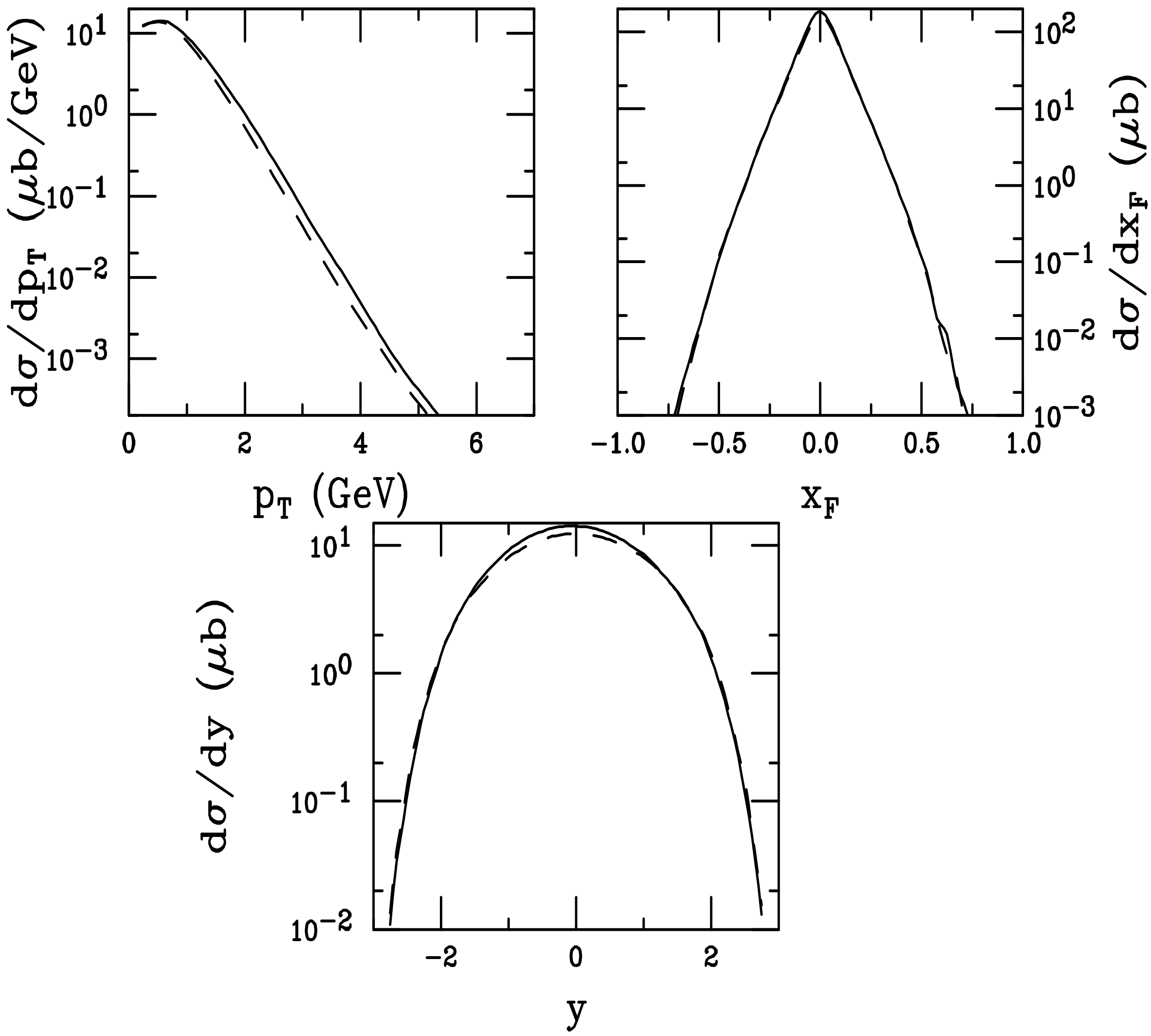

Figure 11: Inclusive NLO c quark production in pp and pA interactions at 800 GeV as a function of p_T, x_F, and y. The p_T distributions are integrated over $x_F > 0$ only. The per nucleon cross section is given for pA interactions. The dashed curves are the pp results while the solid curves are the pA results.

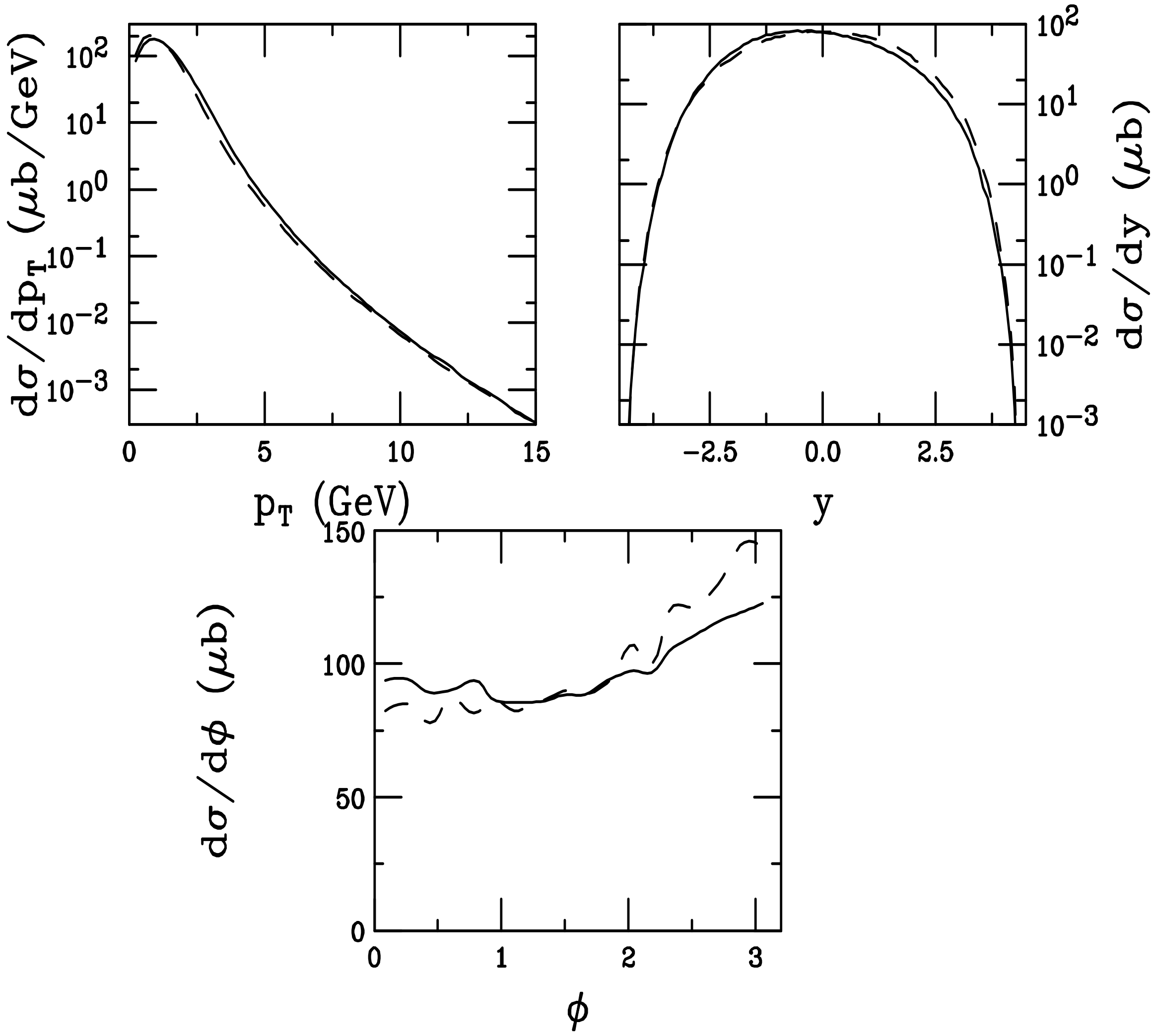

Figure 12: Exclusive NLO $c\overline{c}$ pair production in pp and pA interactions at $\sqrt{s} = 200$ GeV as a function of p_T, y, and ϕ. The per nucleon cross section is given for pA interactions. The dashed curves are the pp results while the solid curves are the pA results.

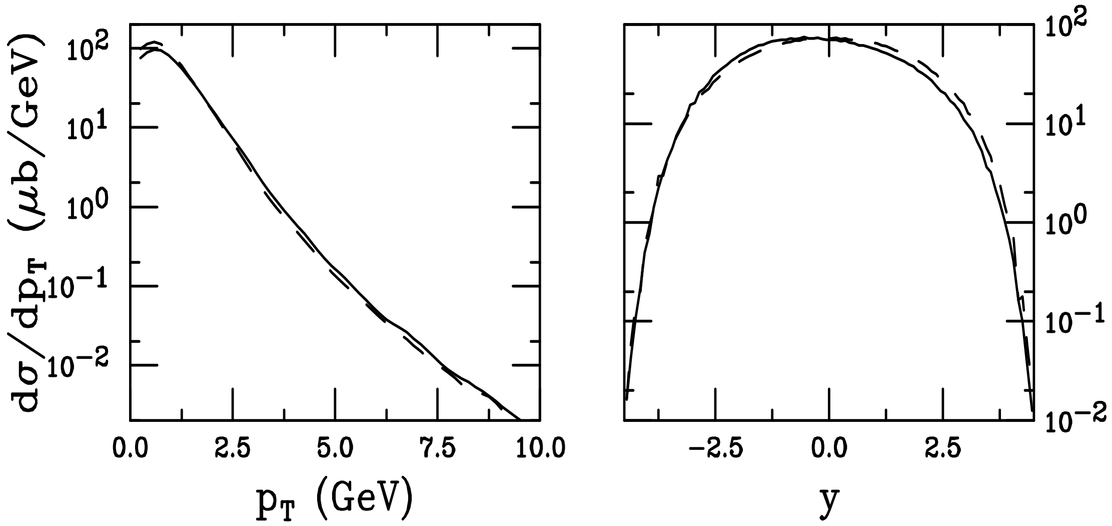

Figure 13: Inclusive NLO c quark production in pp and pA interactions at $\sqrt{s} = 200$ GeV as a function of p_T and y. The p_T distributions are integrated over $x_F > 0$ only. The per nucleon cross section is given for pA interactions. The dashed curves are the pp results while the solid curves are the pA results.

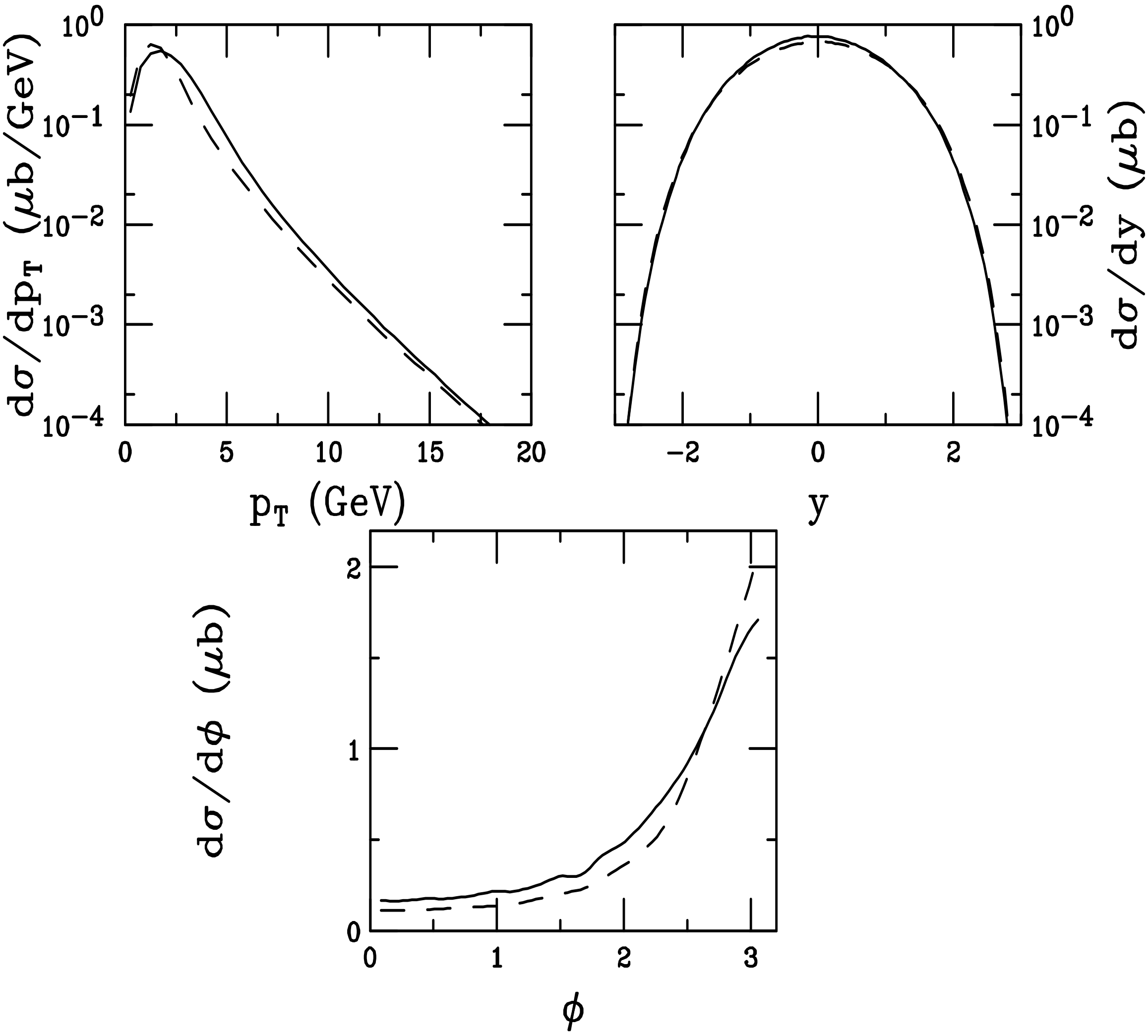

Figure 14: Exclusive NLO $b\bar{b}$ pair production in pp and pA interactions at $\sqrt{s} = 200$ GeV as a function of p_T, y, and ϕ. The per nucleon cross section is given for pA interactions. The dashed curves are the pp results while the solid curves are the pA results.

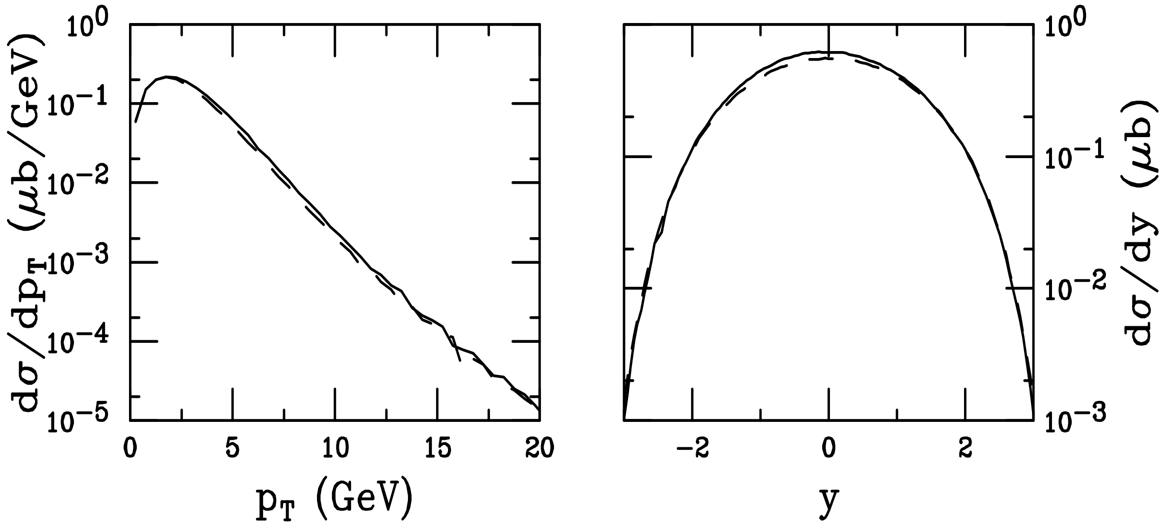

Figure 15: Inclusive NLO b quark production in pp and pA interactions at $\sqrt{s} = 200$ GeV as a function of p_T and y. The p_T distributions are integrated over $x_F > 0$ only. The per nucleon cross section is given for pA interactions. The dashed curves are the pp results while the solid curves are the pA results.

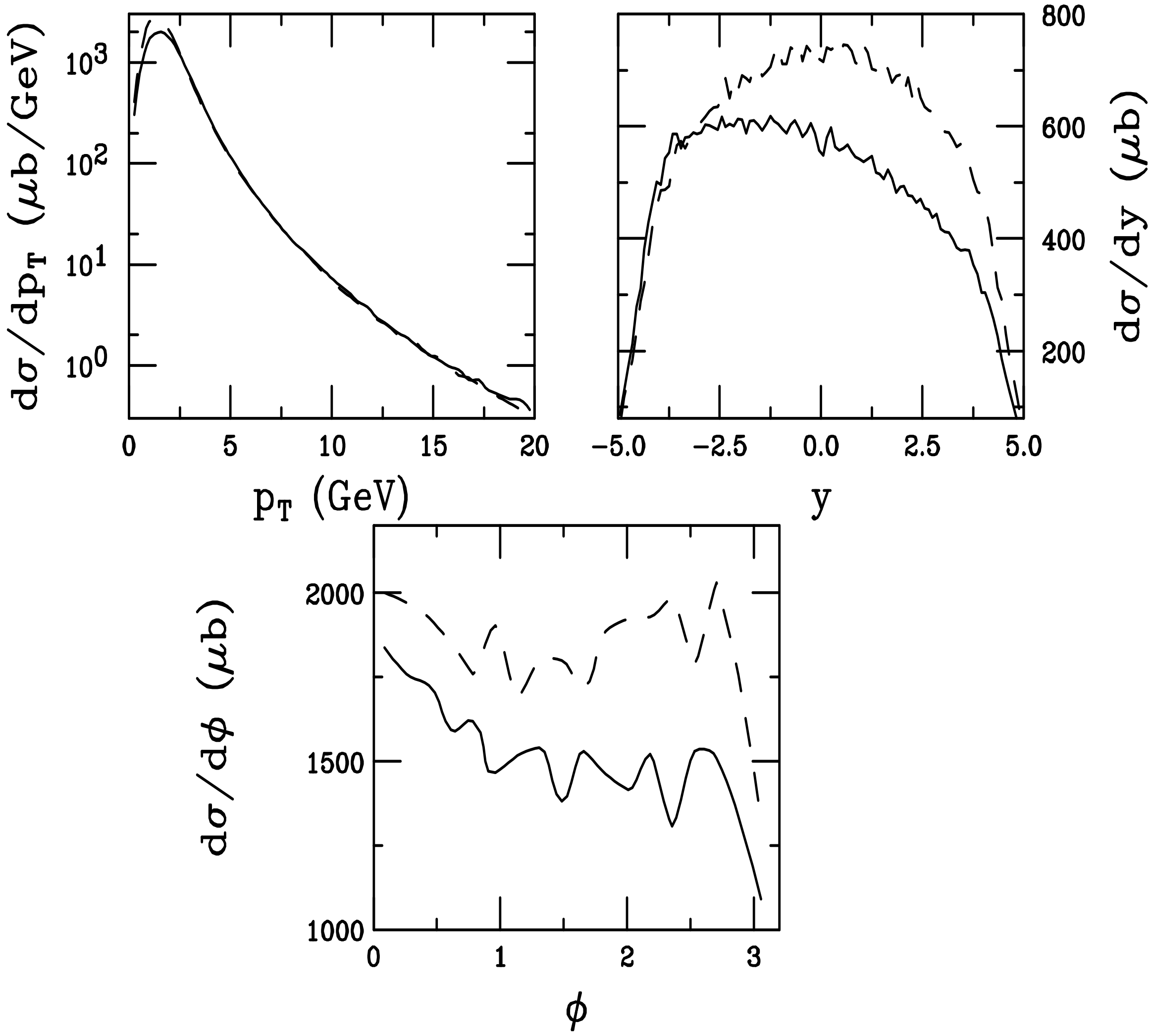

Figure 16: Exclusive NLO $c\overline{c}$ pair production in pp and pA interactions at $\sqrt{s} = 5.5$ TeV as a function of p_T, y, and ϕ. The per nucleon cross section is given for pA interactions. The dashed curves are the pp results while the solid curves are the pA results.

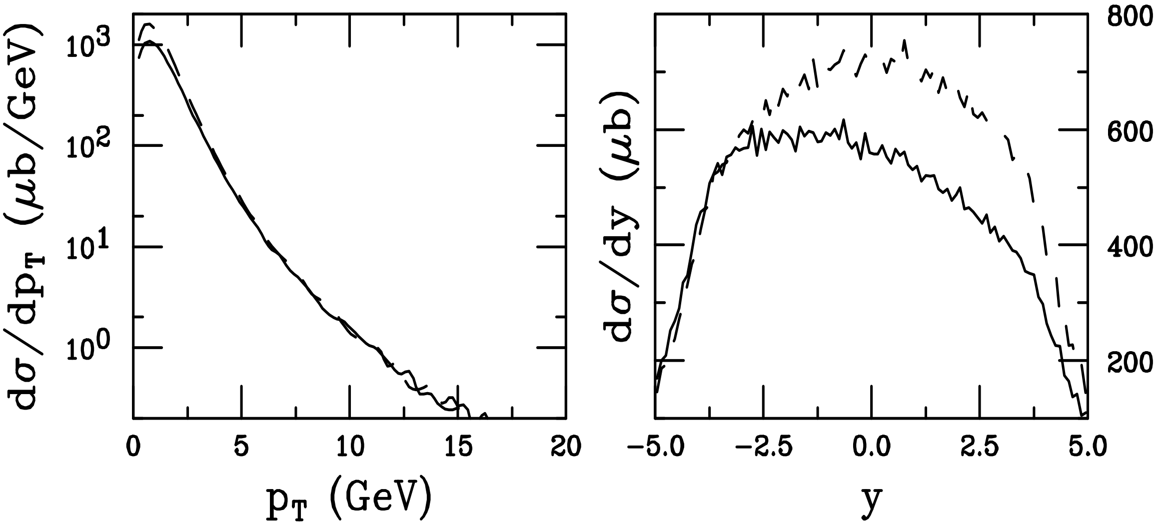

Figure 17: Inclusive NLO c quark production in pp and pA interactions at $\sqrt{s} = 5.5$ TeV as a function of p_T and y. The p_T distributions are integrated over $x_F > 0$ only. The per nucleon cross section is given for pA interactions. The dashed curves are the pp results while the solid curves are the pA results.

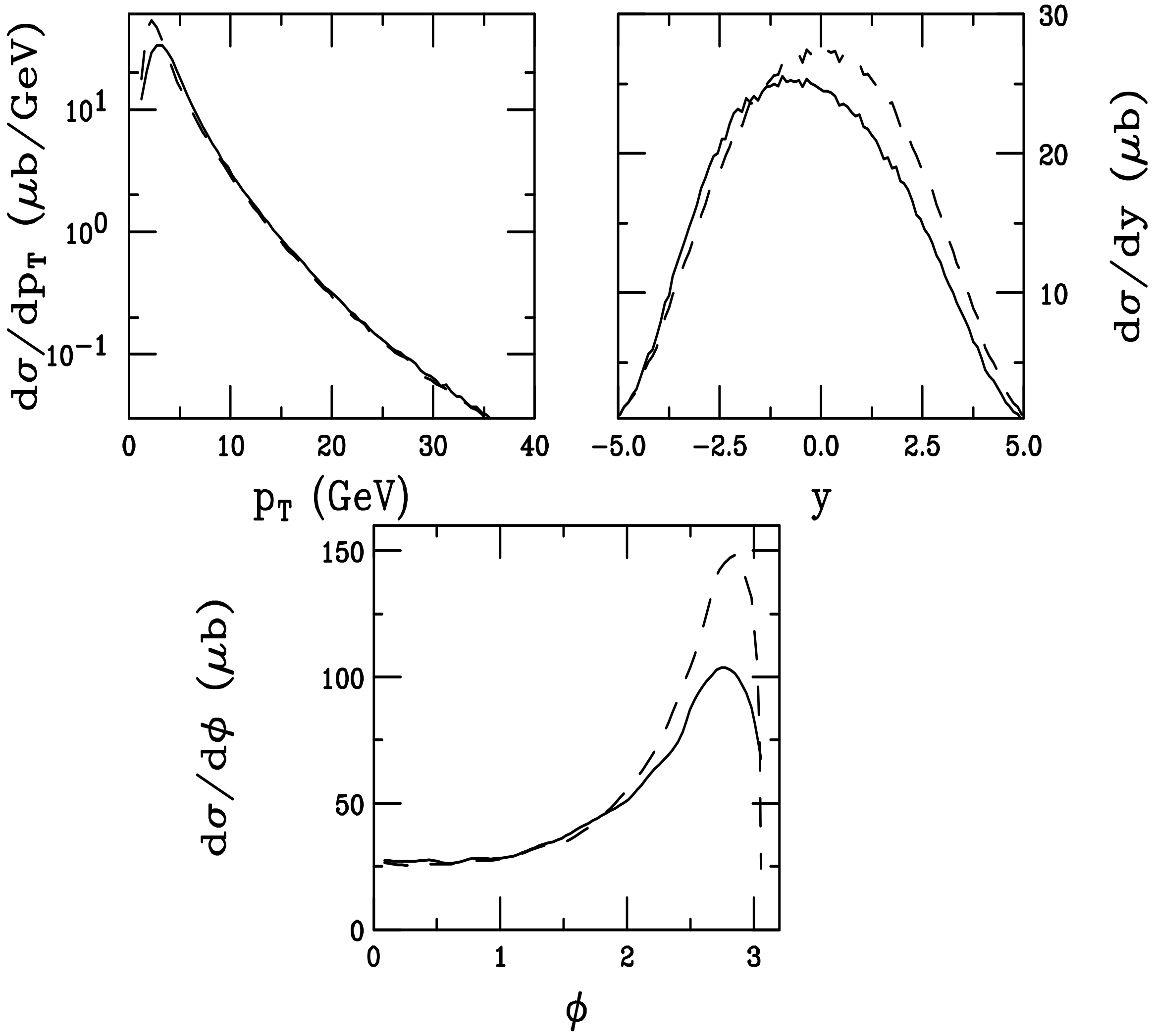

Figure 18: Exclusive NLO $b\overline{b}$ pair production in pp and pA interactions at $\sqrt{s} = 5.5$ TeV as a function of p_T, y, and ϕ. The per nucleon cross section is given for pA interactions. The dashed curves are the pp results while the solid curves are the pA results.

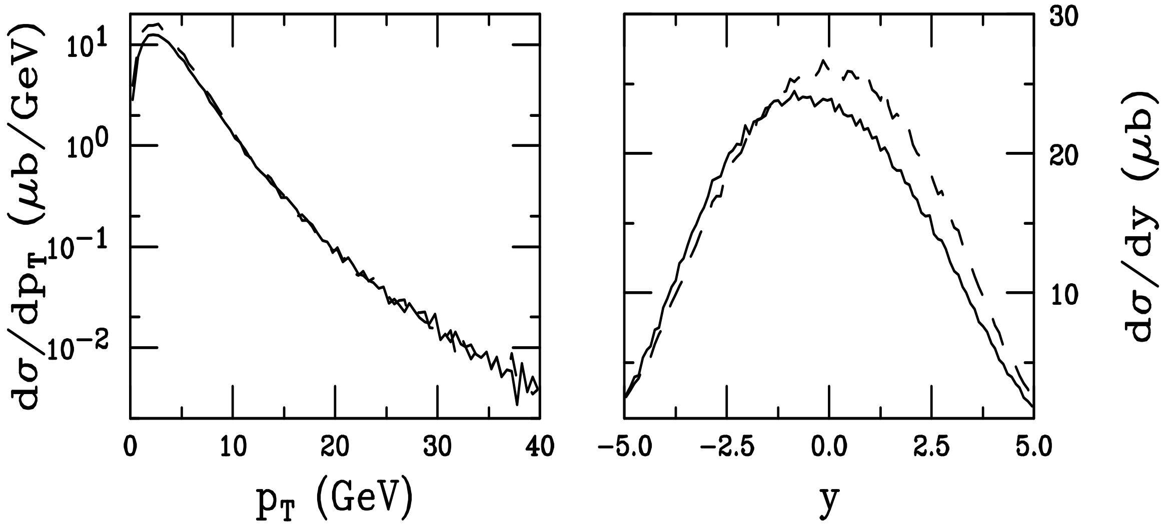

Figure 19: Inclusive NLO b quark production in pp and pA interactions at $\sqrt{s} = 5.5$ TeV as a function of p_T and y. The p_T distributions are integrated over $x_F > 0$ only. The per nucleon cross section is given for pA interactions. The dashed curves are the pp results while the solid curves are the pA results.

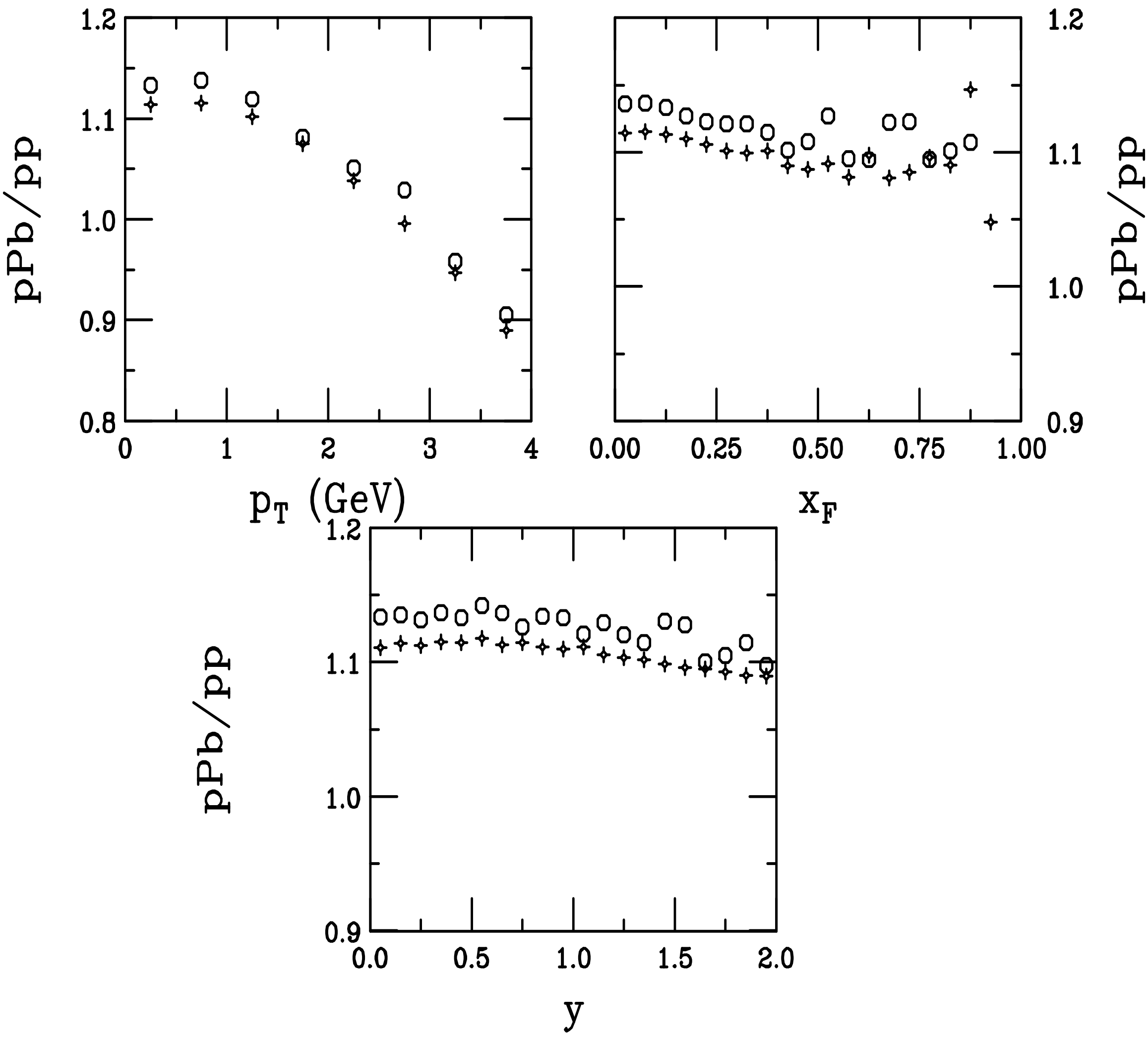

Figure 20: Ratio of c quark production in pA to pp interactions at 158 GeV as a function of p_T, x_F, and y. The crosses are the LO results while the circles are the NLO results.

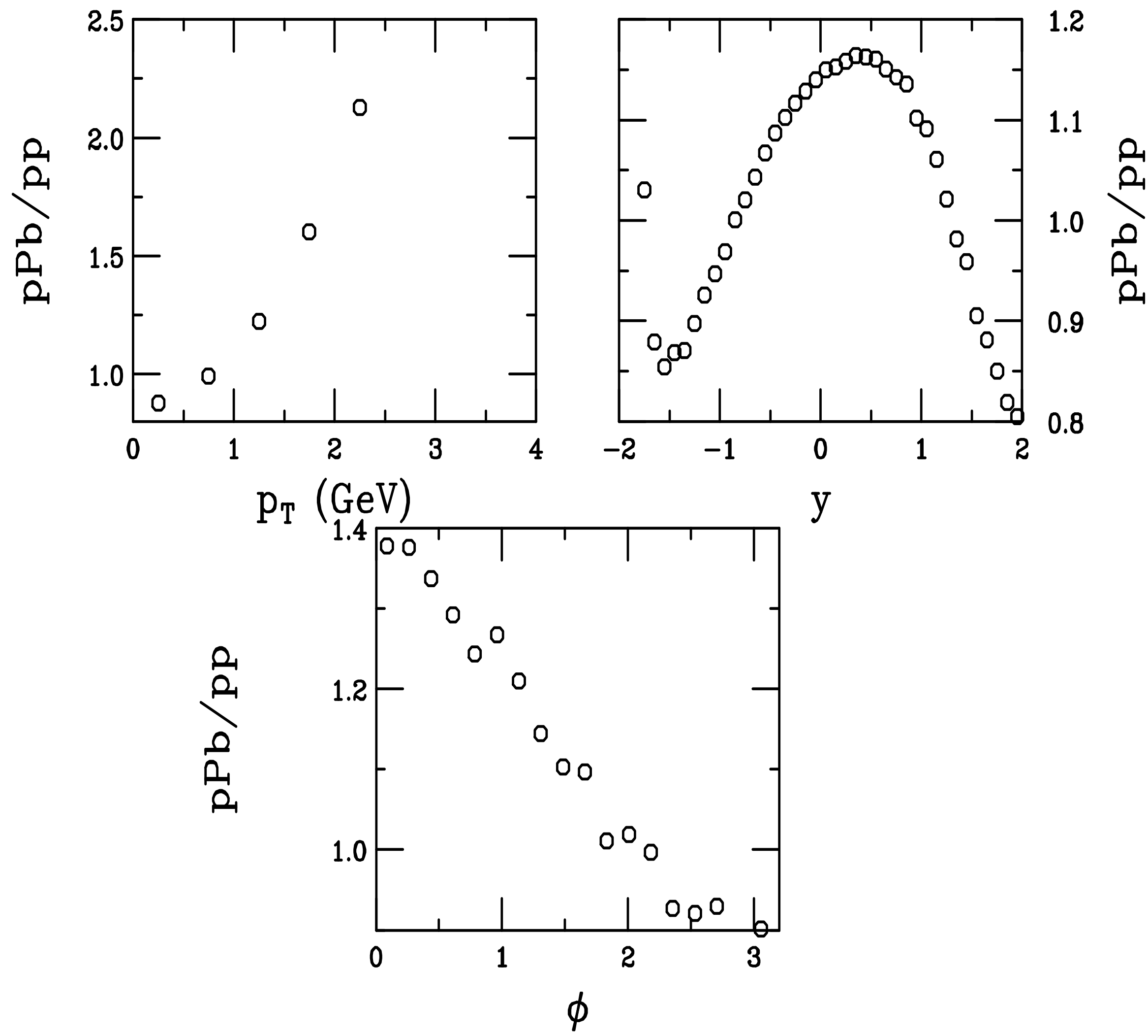

Figure 21: The ratio of pA to pp exclusive NLO $c\overline{c}$ pair production at 158 GeV as a function of p_T, y, and ϕ.

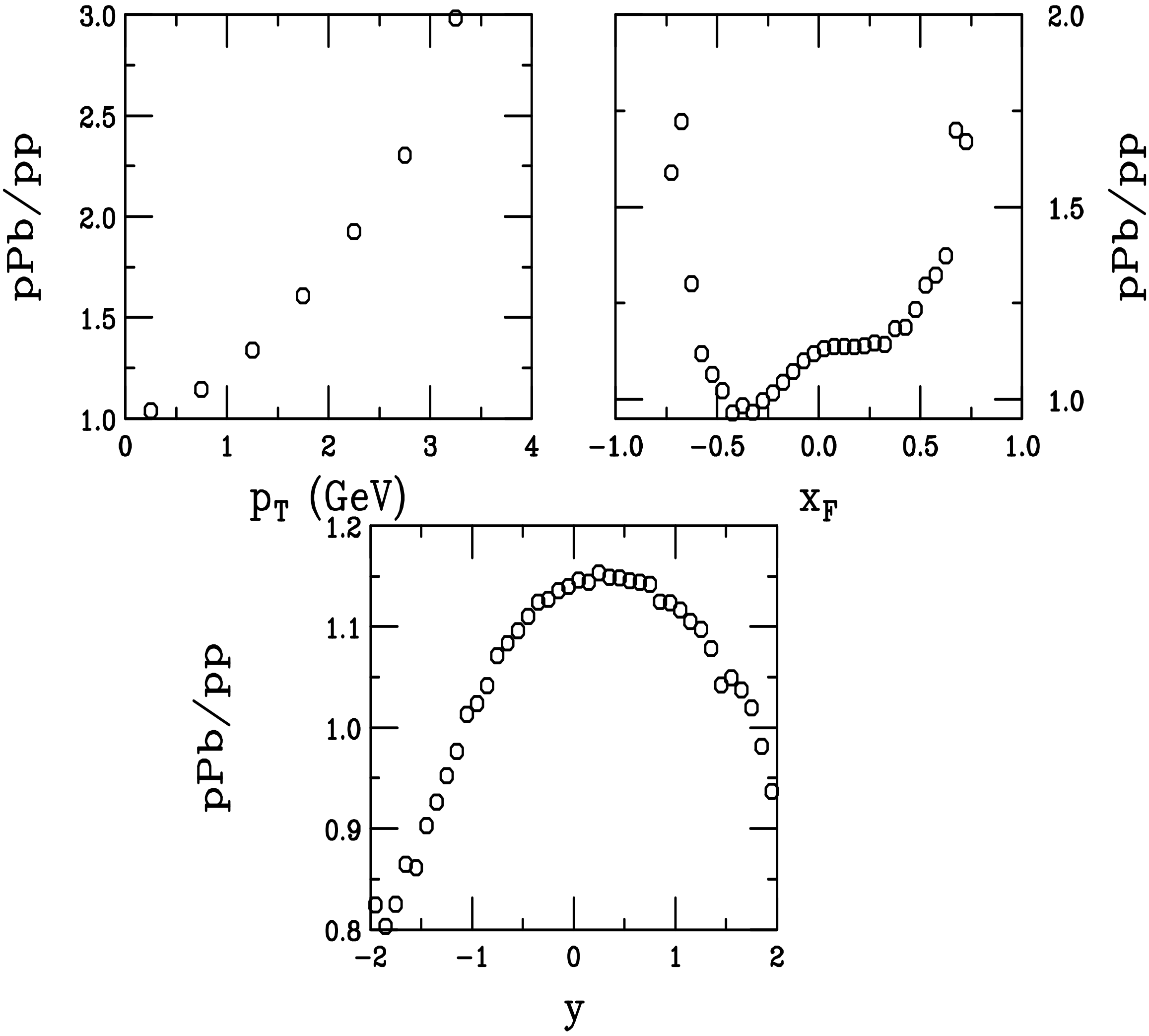

Figure 22: The ratio of pA to pp inclusive NLO c quark production at 158 GeV as a function of p_T, x_F, and y.

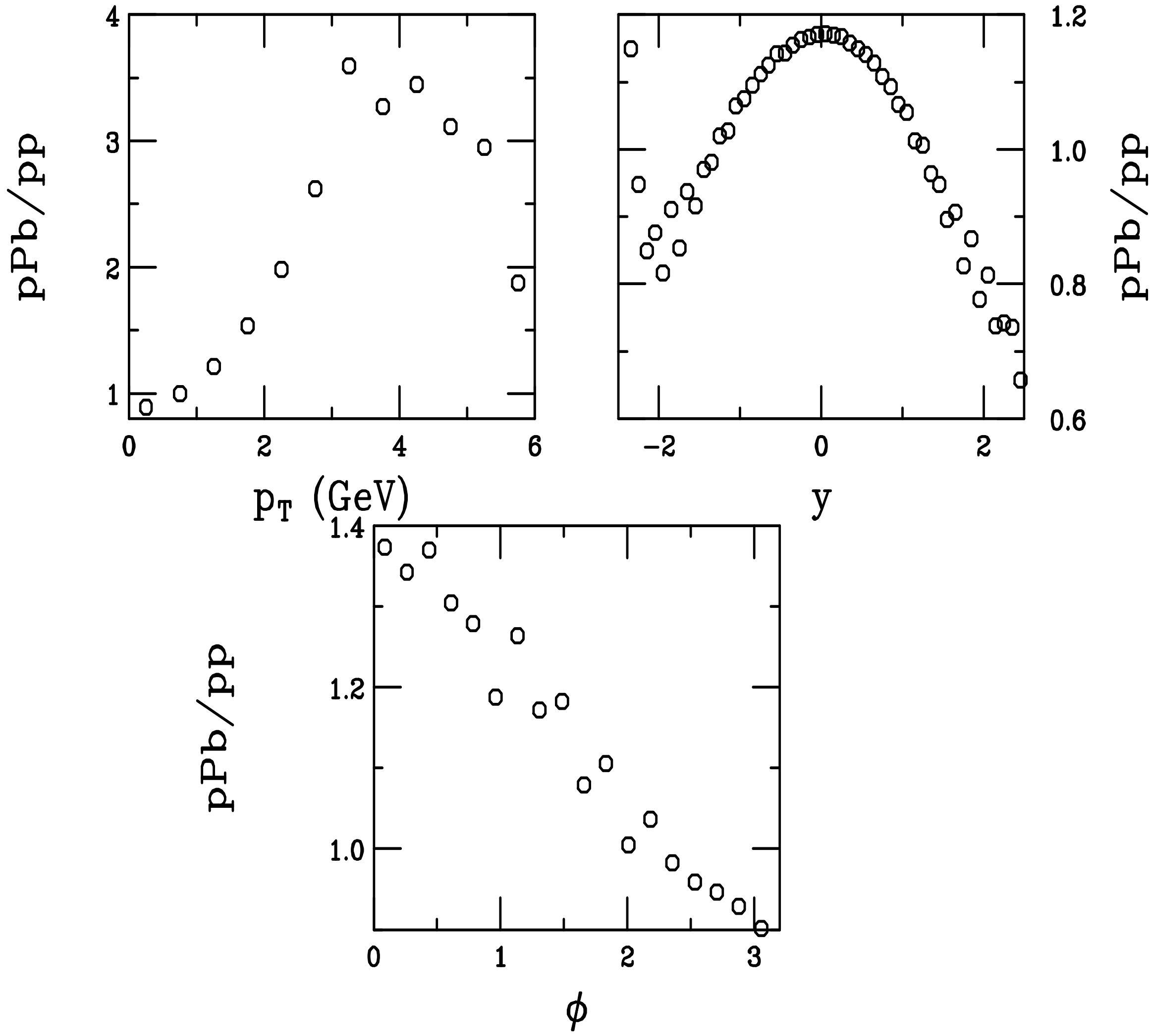

Figure 23: The ratio of pA to pp exclusive NLO $c\overline{c}$ pair production at 450 GeV as a function of p_T, y, and ϕ.

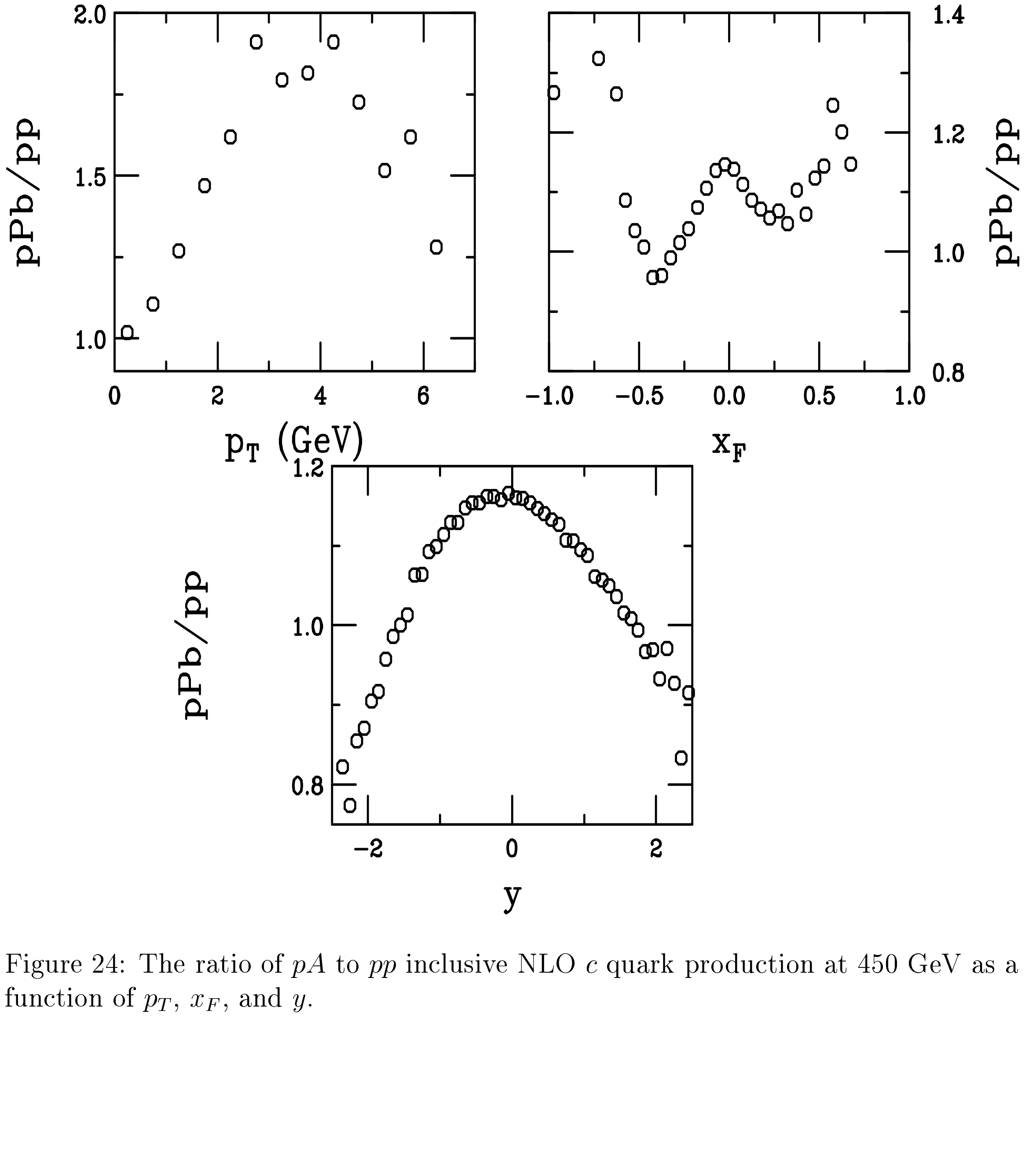

Figure 24: The ratio of pA to pp inclusive NLO c quark production at 450 GeV as a function of p_T, x_F, and y.

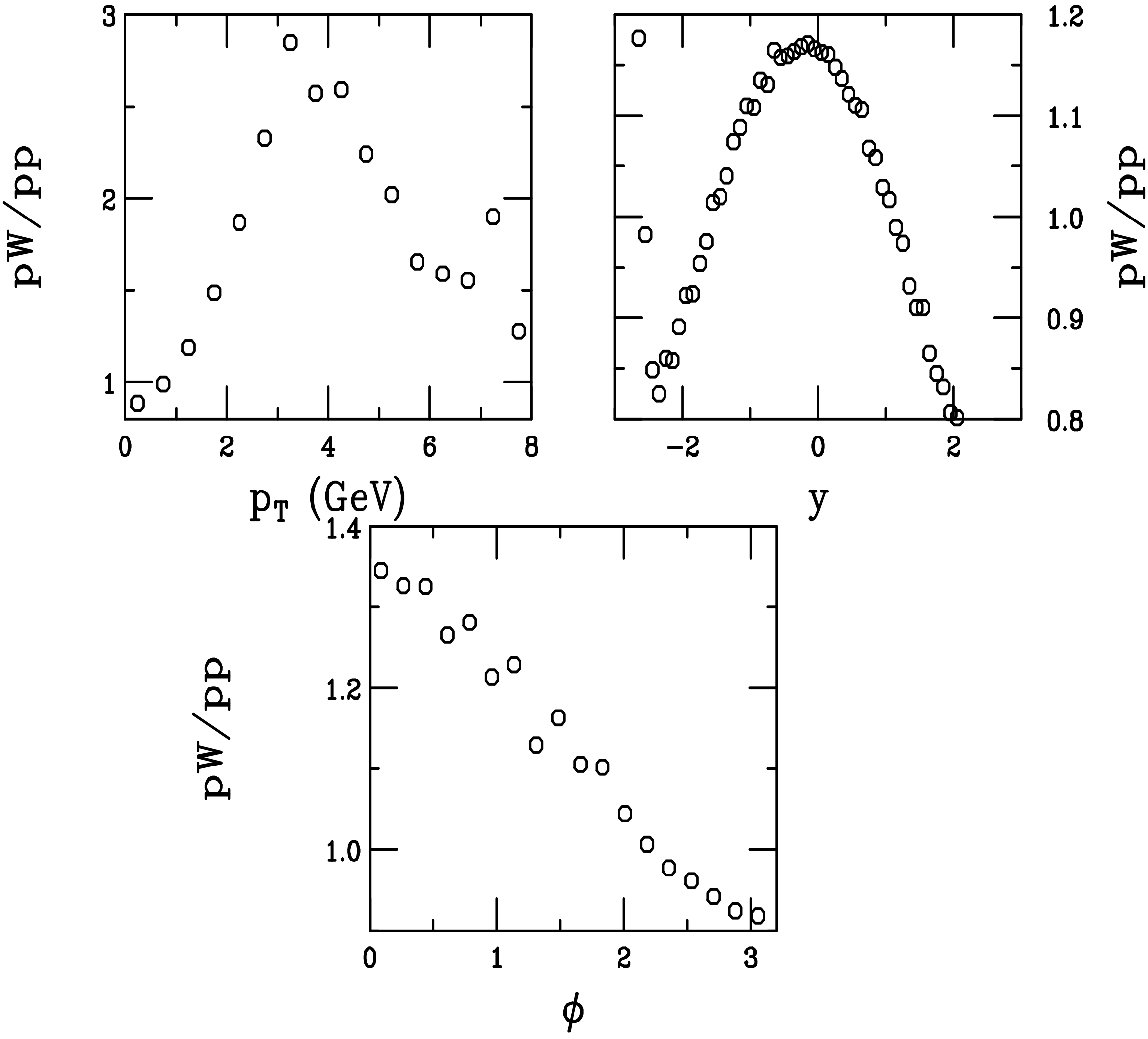

Figure 25: The ratio of pA to pp exclusive NLO $c\overline{c}$ pair production at 800 GeV as a function of p_T, y, and ϕ.

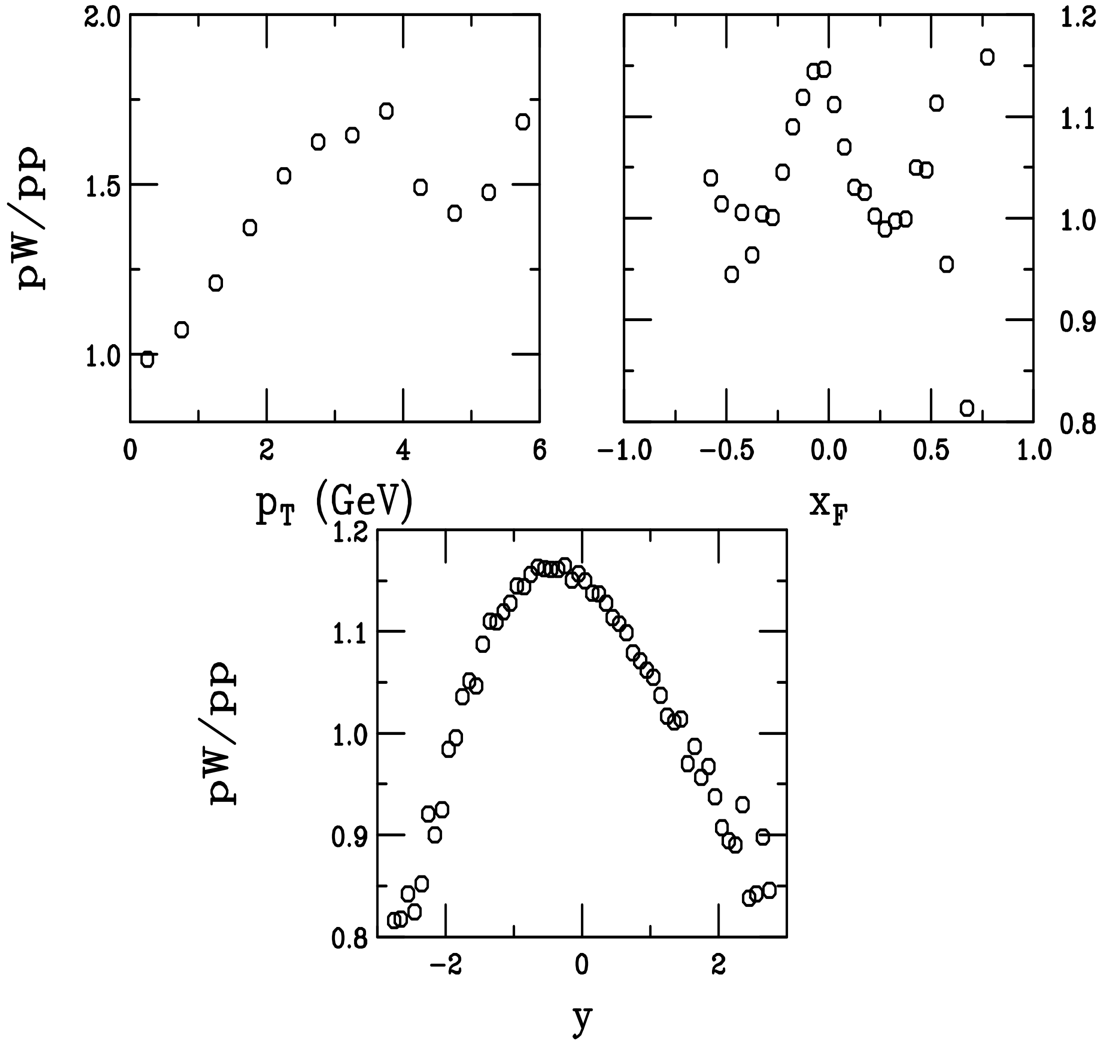

Figure 26: The ratio of pA to pp inclusive NLO c quark production at 800 GeV as a function of p_T, x_F, and y.

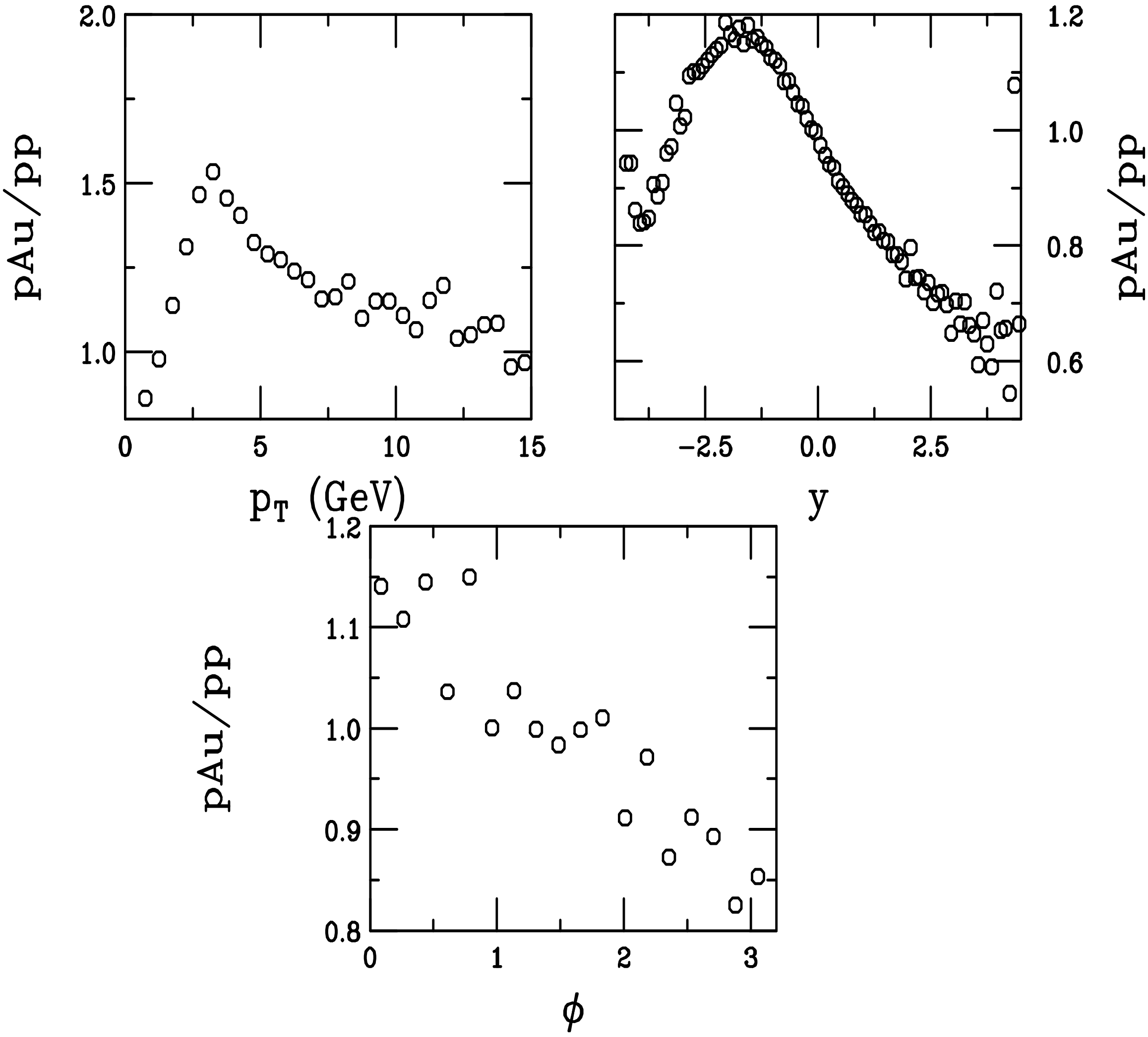

Figure 27: The ratio of pA to pp exclusive NLO $c\overline{c}$ pair production at $\sqrt{s} = 200$ GeV as a function of p_T, y, and ϕ.

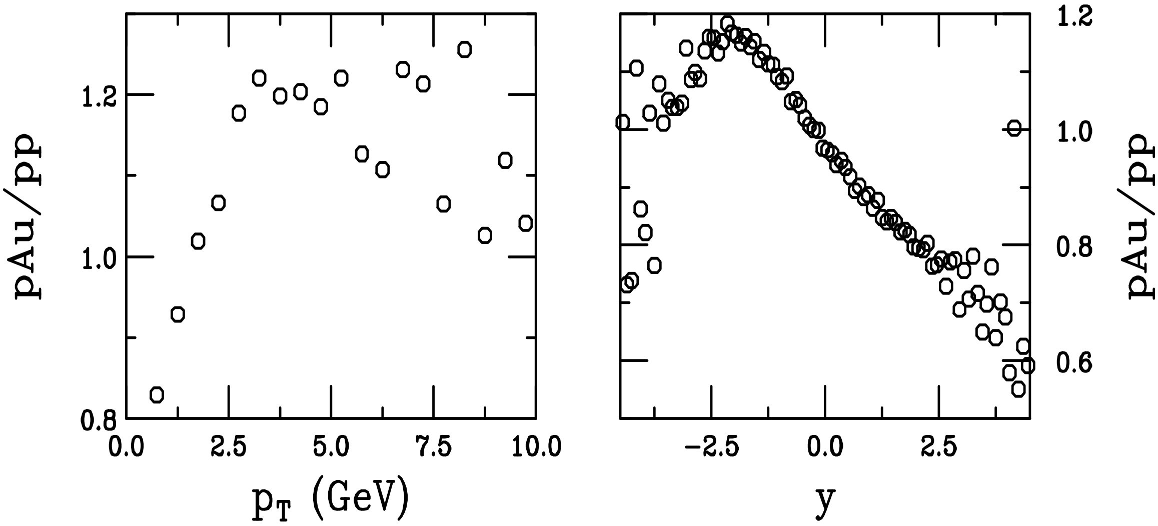

Figure 28: The ratio of pA to pp inclusive NLO c quark production at $\sqrt{s} = 200$ GeV as a function of p_T and y.

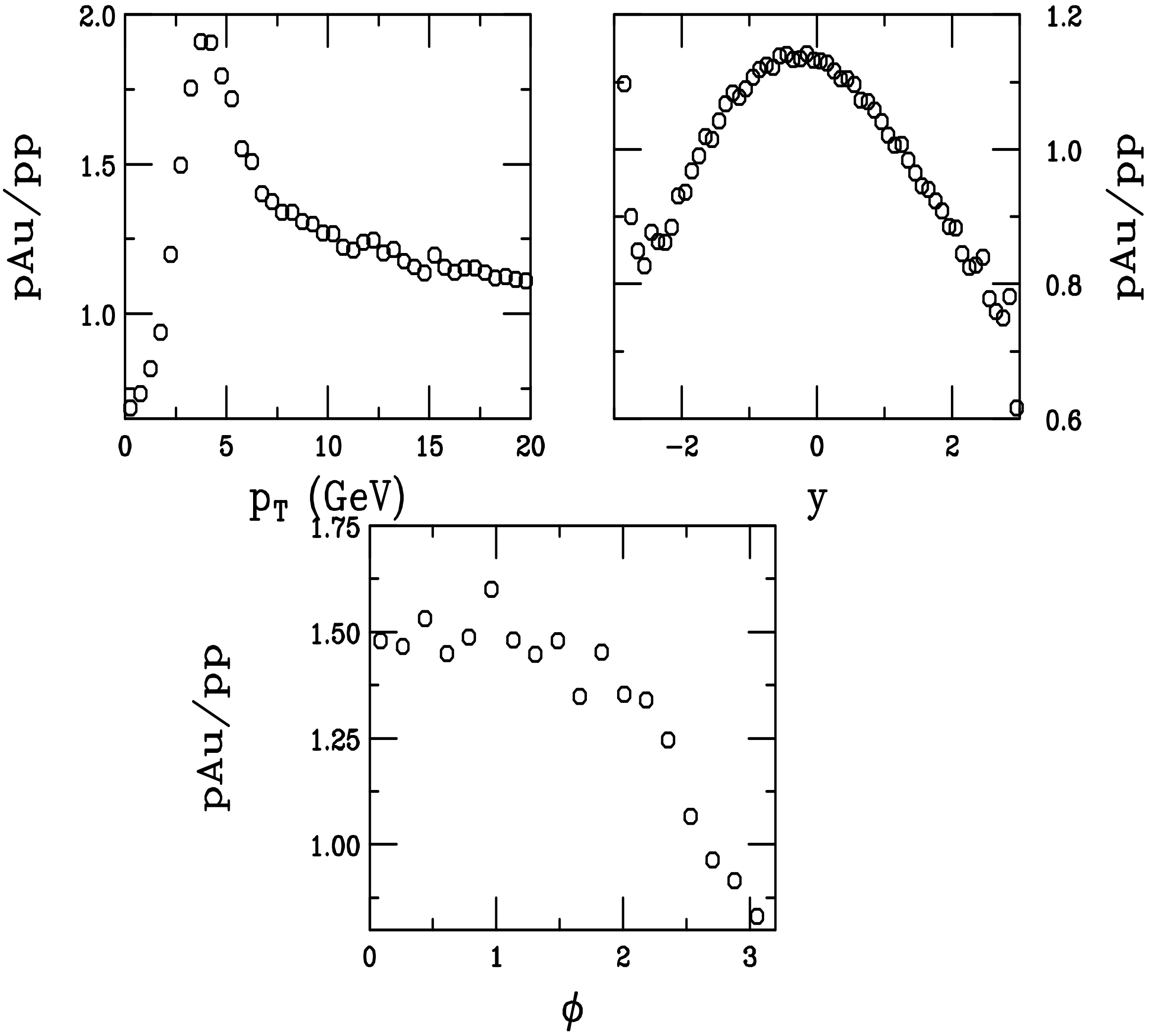

Figure 29: The ratio of pA to pp exclusive NLO $b\overline{b}$ pair production at $\sqrt{s} = 200$ GeV as a function of p_T, y, and ϕ.

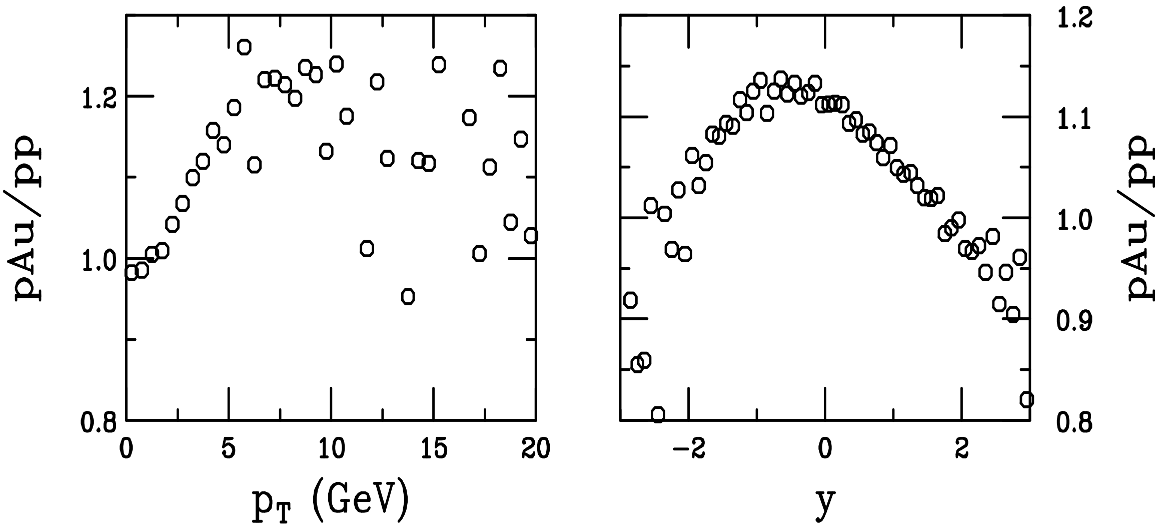

Figure 30: The ratio of pA to pp inclusive NLO c quark production at $\sqrt{s} = 200$ GeV as a function of p_T and y.

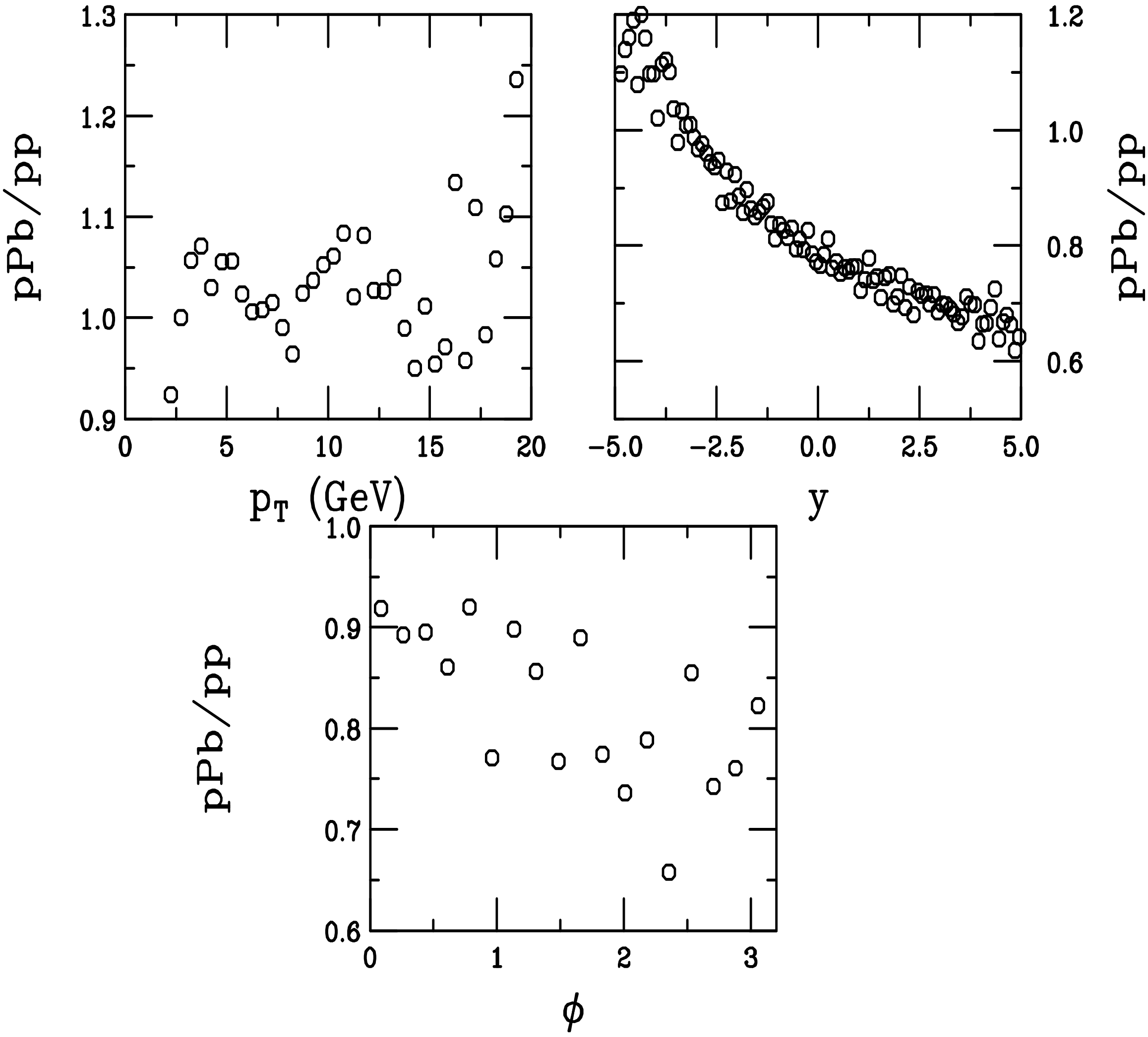

Figure 31: The ratio of pA to pp exclusive NLO $c\overline{c}$ pair production at $\sqrt{s} = 5.5$ TeV as a function of p_T, y, and ϕ.

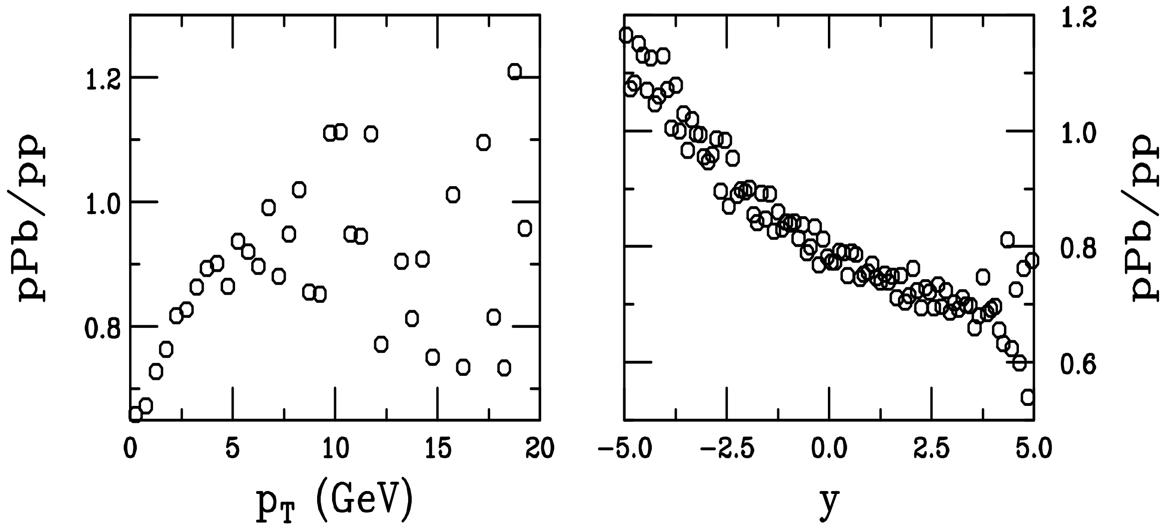

Figure 32: The ratio of pA to pp inclusive NLO c quark production at $\sqrt{s} = 5.5$ TeV as a function of p_T and y.

	$d\sigma_{c\overline{c}}/dp_T$ (nb/GeV)		$d\sigma_c/dp_T$ (nb/GeV)	
p_T (GeV)	pp	pA	pp	pA
0.25	2104.000	1848.000	1970.400	2046.000
0.75	3470.000	3440.000	1669.400	1909.400
1.25	2048.000	2504.000	527.000	705.200
1.75	747.600	1197.000	115.180	185.060
2.25	198.080	421.600	20.100	38.720
2.75	38.140	116.940	3.040	7.006
3.25	5.188	27.220	0.391	1.166
3.75	0.788	3.852	0.044	0.135
4.25	0.107	0.867	0.008	0.017

Table 3: The NLO exclusive $c\overline{c}$ and inclusive single charm p_T distributions for a proton beam of 158 GeV. The exclusive $c\overline{c}$ distributions are integrated over all rapidity while the inclusive single charm p_T distributions are integrated over $x_F > 0$ only. The distributions for pp and pA interactions are both given. The per nucleon cross section is given for pA interactions. Recall that the intrinsic $\langle k_T^2 \rangle$ is 1 GeV^2 for pp interactions and 1.35 GeV^2 for pA interactions.

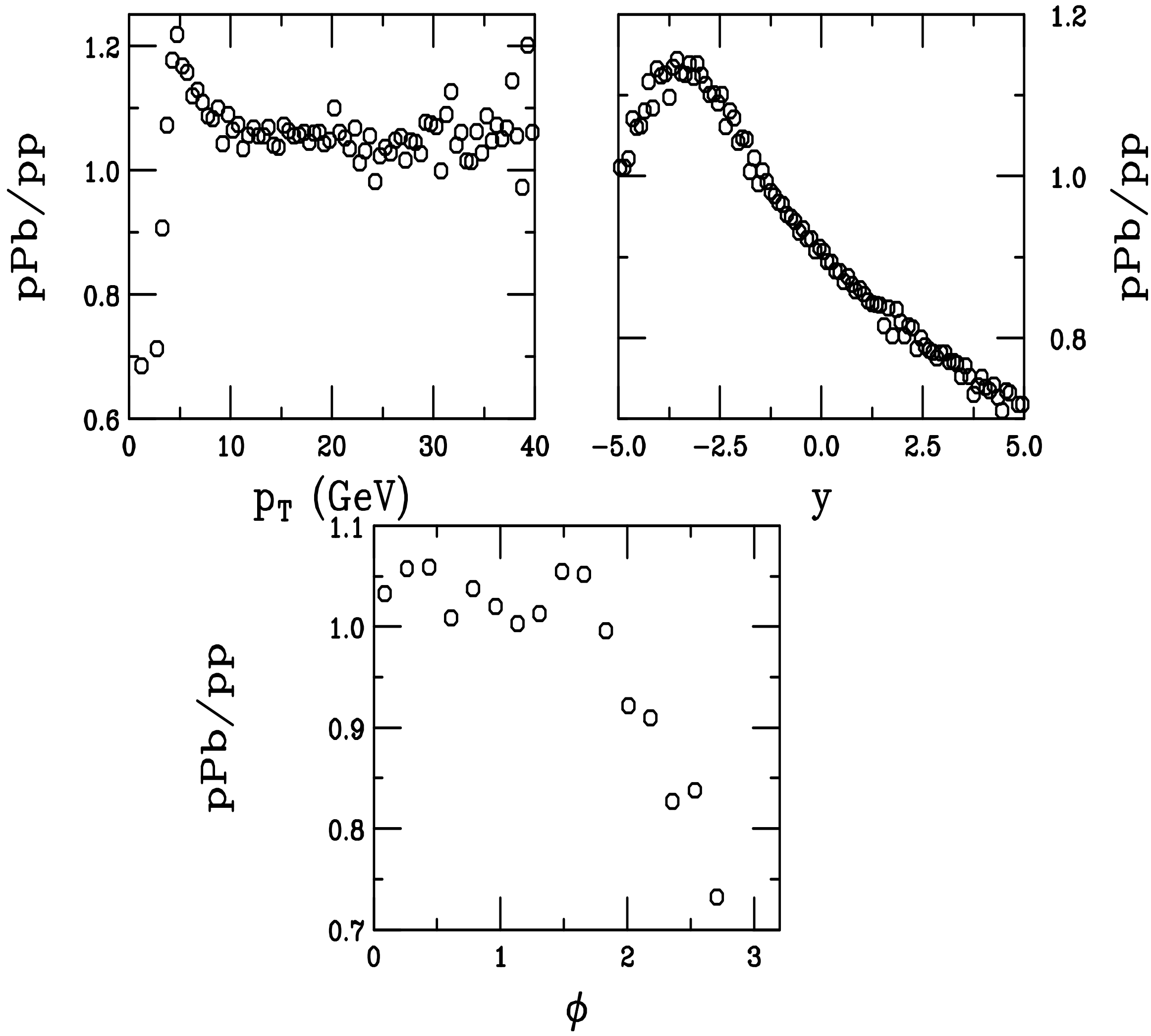

Figure 33: The ratio of pA to pp exclusive NLO $b\overline{b}$ pair production at $\sqrt{s} = 5.5$ TeV as a function of p_T, y, and ϕ.

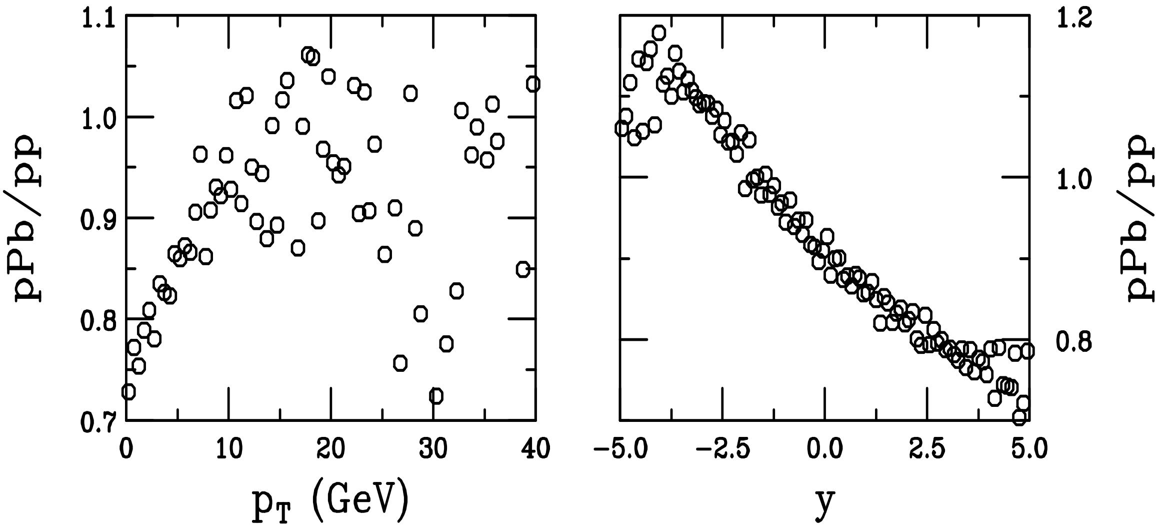

Figure 34: The ratio of pA to pp inclusive NLO b quark production at $\sqrt{s} = 5.5$ TeV as a function of p_T and y.

	$d\sigma_{c\overline{c}}/dp_T$ (nb/GeV)		$d\sigma_c/dp_T$ (nb/GeV)	
p_T (GeV)	pp	pA	pp	pA
0.25	8044.000	7156.000	7214.000	7342.000
0.75	13546.000	13544.000	6704.000	7416.000
1.25	8352.000	10130.000	2456.000	3118.000
1.75	3268.000	5020.000	642.200	943.800
2.25	939.200	1862.600	152.060	246.200
2.75	210.600	552.400	29.800	56.960
3.25	40.220	144.480	6.476	11.616
3.75	8.492	27.780	1.405	2.552
4.25	1.934	6.662	0.313	0.598
4.75	0.476	1.481	0.078	0.135
5.25	0.128	0.378	0.020	0.030
5.75	0.042	0.078	0.004	0.007
6.25	0.011	0.024	0.001	0.001

Table 4: The NLO exclusive $c\overline{c}$ and inclusive single charm p_T distributions for a proton beam of 450 GeV. The exclusive $c\overline{c}$ distributions are integrated over all rapidity while the inclusive single charm p_T distributions are integrated over $x_F > 0$ only. The distributions for pp and pA interactions are both given. The per nucleon cross section is given for pA interactions. Recall that the intrinsic $\langle k_T^2 \rangle$ is 1 GeV^2 for pp interactions and 1.35 GeV^2 for pA interactions.

p_T (GeV)	$d\sigma_{c\overline{c}}/dp_T$ (nb/GeV) pp	$d\sigma_{c\overline{c}}/dp_T$ (nb/GeV) pA	$d\sigma_c/dp_T$ (nb/GeV) pp	$d\sigma_c/dp_T$ (nb/GeV) pA
0.25	14168.000	12530.000	12486.000	12300.000
0.75	24160.000	23880.000	12100.000	12952.000
1.25	15346.000	18216.000	4788.000	5790.000
1.75	6266.000	9312.000	1383.600	1899.800
2.25	1902.400	3558.000	356.200	543.000
2.75	480.600	1119.000	86.240	140.140
3.25	109.220	311.200	21.080	34.680
3.75	27.720	71.280	5.578	9.570
4.25	7.820	20.280	1.661	2.478
4.75	2.456	5.510	0.493	0.698
5.25	0.787	1.591	0.166	0.245
5.75	0.297	0.491	0.048	0.081
6.25	0.111	0.176	0.018	0.021
6.75	0.044	0.068	0.005	0.007
7.25	0.014	0.027	0.002	0.003

Table 5: The NLO exclusive $c\overline{c}$ and inclusive single charm p_T distributions for a proton beam of 800 GeV. The exclusive $c\overline{c}$ distributions are integrated over all rapidity while the inclusive single charm p_T distributions are integrated over $x_F > 0$ only. The distributions for pp and pA interactions are both given. The per nucleon cross section is given for pA interactions. Recall that the intrinsic $\langle k_T^2 \rangle$ is 1 GeV^2 for pp interactions and 1.35 GeV^2 for pA interactions.

	$d\sigma_{c\overline{c}}/dp_T$ (μb/GeV)		$d\sigma_c/dp_T$ (μb/GeV)	
p_T (GeV)	pp	pA	pp	pA
0.25	106.640	84.080	98.400	75.740
0.75	204.800	176.440	113.660	94.220
1.25	162.540	158.960	60.160	55.860
1.75	89.340	101.580	25.480	25.960
2.25	38.820	50.860	10.330	11.016
2.75	15.744	23.080	4.082	4.806
3.25	6.390	9.796	1.612	1.967
3.75	2.918	4.246	0.752	0.902
4.25	1.433	2.014	0.377	0.454
4.75	0.765	1.013	0.185	0.220
5.25	0.421	0.543	0.101	0.123
5.75	0.243	0.310	0.058	0.066
6.25	0.145	0.180	0.034	0.038
6.75	0.091	0.110	0.021	0.026
7.25	0.058	0.067	0.013	0.015
7.75	0.038	0.044	0.008	0.009
8.25	0.024	0.029	0.005	0.006
8.75	0.017	0.019	0.004	0.004
9.25	0.011	0.013	0.002	0.003
9.75	0.008	0.009	0.002	0.002

Table 6: The NLO exclusive $c\overline{c}$ and inclusive single charm p_T distributions for collisions at $\sqrt{s} = 200$ GeV. The exclusive $c\overline{c}$ distributions are integrated over all rapidity while the inclusive single charm p_T distributions are integrated over $x_F > 0$ only. The distributions for pp and pA interactions are both given. The per nucleon cross section is given for pA interactions. Recall that the intrinsic $\langle k_T^2 \rangle$ is 1 GeV^2 for pp interactions and 1.35 GeV^2 for pA interactions.

p_T (GeV)	$d\sigma_{c\overline{c}}/dp_T$ (μb/GeV) pp	pA	$d\sigma_c/dp_T$ (μb/GeV) pp	pA
0.25	407.800	301.400	1123.800	740.400
0.75	1791.000	1221.600	1604.400	1078.800
1.25	2732.000	1921.200	1202.200	875.000
1.75	2464.000	1932.400	755.600	577.000
2.25	1615.200	1492.800	428.800	350.800
2.75	938.400	939.000	242.200	200.400
3.25	540.200	570.800	143.700	124.140
3.75	324.200	347.200	85.380	76.260
4.25	207.800	214.000	53.500	48.260
4.75	133.820	141.280	36.640	31.680
5.25	92.220	97.380	23.160	21.700
5.75	65.940	67.480	16.696	15.368
6.25	47.900	48.180	11.192	10.042
6.75	35.580	35.880	8.354	8.282
7.25	26.420	26.820	6.568	5.788
7.75	20.400	20.200	4.900	4.650
8.25	16.306	15.728	3.378	3.446
8.75	12.646	12.958	2.886	2.468
9.25	9.750	10.112	2.316	1.973
9.75	7.740	8.150	1.631	1.812
10.25	6.162	6.538	1.267	1.411
10.75	5.046	5.468	1.159	1.099
11.25	4.216	4.304	1.024	0.968
11.75	3.512	3.798	0.660	0.733
12.25	2.850	2.928	0.719	0.554
12.75	2.474	2.540	0.406	0.580
13.25	2.016	2.096	0.386	0.350
13.75	1.881	1.862	0.430	0.349
14.25	1.601	1.522	0.283	0.257
14.75	1.280	1.296	0.322	0.241
15.25	1.200	1.146	0.203	0.271
15.75	1.011	0.982	0.176	0.178
16.25	0.799	0.905	0.223	0.164
16.75	0.752	0.720	0.117	0.166
17.25	0.647	0.718	0.102	0.111
17.75	0.576	0.566	0.128	0.104

Table 7: The NLO exclusive $c\overline{c}$ and inclusive single charm p_T distributions for collisions at $\sqrt{s} = 5.5$ TeV. The exclusive $c\overline{c}$ distributions are integrated over all rapidity while the inclusive single charm p_T distributions are integrated over $x_F > 0$ only. The distributions for pp and pA interactions are both given. The per nucleon cross section is given for pA interactions. Recall that the intrinsic $\langle k_T^2 \rangle$ is 1 GeV^2 for pp interactions and 1.35 GeV^2 for pA interactions.

p_T (GeV)	$d\sigma_{b\overline{b}}/dp_T$ (nb/GeV) pp	pA	$d\sigma_b/dp_T$ (nb/GeV) pp	pA
0.25	196.260	134.740	60.320	59.260
0.75	512.400	375.200	152.900	150.680
1.25	632.600	516.800	199.820	200.800
1.75	583.400	547.400	218.200	220.200
2.25	411.800	493.600	205.200	213.800
2.75	271.200	406.000	176.080	188.020
3.25	167.880	294.400	143.840	158.220
3.75	108.580	207.400	112.120	125.600
4.25	72.620	138.440	83.480	96.660
4.75	51.360	92.200	64.340	73.340
5.25	36.100	62.080	44.880	53.240
5.75	26.980	41.860	32.120	40.500
6.25	20.000	30.180	24.240	27.040
6.75	15.304	21.440	16.774	20.480
7.25	11.450	15.744	11.866	14.502
7.75	8.794	11.774	8.878	10.784
8.25	6.684	8.946	6.260	7.496
8.75	5.188	6.792	4.486	5.542
9.25	4.046	5.260	3.276	4.020
9.75	3.178	4.036	2.472	2.798
10.25	2.464	3.124	1.741	2.158
10.75	1.970	2.408	1.340	1.575
11.25	1.572	1.906	0.891	1.168
11.75	1.220	1.512	0.810	0.820
12.25	0.969	1.209	0.567	0.691
12.75	0.772	0.929	0.448	0.503
13.25	0.625	0.759	0.301	0.432
13.75	0.511	0.601	0.276	0.263
14.25	0.413	0.478	0.187	0.210
14.75	0.342	0.388	0.166	0.185
15.25	0.266	0.318	0.123	0.152
15.75	0.217	0.250	0.112	0.088
16.25	0.176	0.201	0.043	0.079
16.75	0.142	0.164	0.060	0.070
17.25	0.116	0.134	0.051	0.051
17.75	0.095	0.108	0.033	0.037

Table 8: The NLO exclusive $b\overline{b}$ and inclusive single bottom p_T distributions for collisions at $\sqrt{s} = 200$ GeV. The exclusive $b\overline{b}$ distributions are integrated over all rapidity while the inclusive single bottom p_T distributions are integrated over $x_F > 0$ only. The distributions for pp and pA interactions are both given. The per nucleon cross section is given for pA interactions. Recall that the intrinsic $\langle k_T^2 \rangle$ is 1 GeV^2 for pp interactions and 2.57 GeV^2 for pA interactions.

p_T (GeV)	$d\sigma_{b\overline{b}}/dp_T$ (μb/GeV) pp	pA	$d\sigma_b/dp_T$ (μb/GeV) pp	pA
1.25	17.738	12.142	13.646	10.286
1.75	45.340	20.480	15.568	12.280
2.25	53.480	29.200	15.502	12.538
2.75	46.660	33.260	15.890	12.408
3.25	36.540	33.120	13.544	11.308
3.75	27.760	29.760	12.574	10.390
4.25	21.680	25.520	10.944	9.006
4.75	16.842	20.520	8.946	7.738
5.25	13.938	16.272	7.910	6.802
5.75	11.326	13.108	6.424	5.606
6.25	9.462	10.594	5.540	4.798
6.75	7.872	8.888	4.524	4.096
7.25	6.600	7.318	3.656	3.520
7.75	5.664	6.156	3.128	2.696
8.25	4.798	5.192	2.616	2.374
8.75	4.112	4.520	2.154	2.004
9.25	3.614	3.768	1.829	1.686
9.75	3.096	3.372	1.502	1.444
10.25	2.672	2.844	1.279	1.187
10.75	2.334	2.504	1.061	1.078
11.25	2.094	2.166	0.904	0.827
11.75	1.821	1.923	0.741	0.756
12.25	1.586	1.693	0.645	0.613
12.75	1.430	1.509	0.608	0.545
13.25	1.239	1.308	0.520	0.491
13.75	1.107	1.184	0.478	0.420
14.25	0.985	1.025	0.387	0.383
14.75	0.903	0.935	0.344	0.307
15.25	0.775	0.831	0.302	0.307
15.75	0.698	0.741	0.261	0.270
16.25	0.645	0.680	0.202	0.232
16.75	0.572	0.605	0.207	0.180
17.25	0.518	0.550	0.183	0.182
17.75	0.464	0.485	0.156	0.166

Table 9: The NLO exclusive $b\overline{b}$ and inclusive single bottom p_T distributions for collisions at $\sqrt{s} = 5.5$ TeV. The exclusive $b\overline{b}$ distributions are integrated over all rapidity while the inclusive single bottom p_T distributions are integrated over $x_F > 0$ only. The distributions for pp and pA interactions are both given. The per nucleon cross section is given for pA interactions. Recall that the intrinsic $\langle k_T^2 \rangle$ is 1 GeV^2 for pp interactions and 2.57 GeV^2 for pA interactions.

	$d\sigma_{c\overline{c}}/dy$ (μb)		$d\sigma_c/dy$ (μb)	
y (GeV)	pp	pA	pp	pA
-1.85	0.000	0.000	0.017	0.014
-1.65	0.009	0.008	0.084	0.072
-1.45	0.069	0.060	0.247	0.223
-1.25	0.243	0.218	0.530	0.505
-1.05	0.601	0.569	0.888	0.900
-0.85	1.131	1.132	1.295	1.349
-0.65	1.707	1.781	1.699	1.841
-0.45	2.237	2.431	2.009	2.230
-0.25	2.642	2.951	2.254	2.541
-0.05	2.834	3.231	2.346	2.674
0.05	2.828	3.252	2.340	2.682
0.25	2.644	3.063	2.248	2.593
0.45	2.238	2.602	2.011	2.309
0.65	1.710	1.968	1.692	1.936
0.85	1.129	1.282	1.300	1.462
1.05	0.600	0.655	0.885	0.988
1.25	0.243	0.248	0.532	0.584
1.45	0.069	0.066	0.250	0.261
1.65	0.009	0.008	0.083	0.086
1.85	0.000	0.000	0.017	0.017

Table 10: The NLO exclusive $c\overline{c}$ and inclusive single charm y distributions for a proton beam of 158 GeV. The distributions for pp and pA interactions are both given. The per nucleon cross section is given for pA interactions. Recall that the intrinsic $\langle k_T^2 \rangle$ is 1 GeV^2 for pp interactions and 1.35 GeV^2 for pA interactions.

	$d\sigma_{c\overline{c}}/dy$ (μb)		$d\sigma_c/dy$ (μb)	
y (GeV)	pp	pA	pp	pA
-2.25	0.004	0.004	0.085	0.066
-2.05	0.043	0.038	0.301	0.262
-1.85	0.210	0.192	0.708	0.648
-1.65	0.604	0.566	1.365	1.346
-1.45	1.367	1.326	2.214	2.243
-1.25	2.389	2.437	3.158	3.360
-1.05	3.719	3.960	4.162	4.572
-0.85	5.147	5.639	5.200	5.870
-0.65	6.516	7.329	6.102	7.002
-0.45	7.712	8.813	6.783	7.824
-0.25	8.536	9.930	7.319	8.505
-0.05	8.998	10.530	7.506	8.750
0.05	8.998	10.540	7.529	8.736
0.25	8.534	9.964	7.284	8.406
0.45	7.702	8.851	6.807	7.761
0.65	6.507	7.344	6.071	6.840
0.85	5.152	5.632	5.193	5.743
1.05	3.722	3.925	4.178	4.543
1.25	2.387	2.402	3.149	3.327
1.45	1.367	1.295	2.176	2.254
1.65	0.605	0.548	1.394	1.405
1.85	0.211	0.183	0.710	0.686
2.05	0.043	0.035	0.292	0.272
2.25	0.004	0.003	0.083	0.077

Table 11: The NLO exclusive $c\overline{c}$ and inclusive single charm y distributions for a proton beam of 450 GeV. The distributions for pp and pA interactions are both given. The per nucleon cross section is given for pA interactions. Recall that the intrinsic $\langle k_T^2 \rangle$ is 1 GeV^2 for pp interactions and 1.35 GeV^2 for pA interactions.

	$d\sigma_{c\overline{c}}/dy$ (μb)		$d\sigma_c/dy$ (μb)	
y (GeV)	pp	pA	pp	pA
-2.45	0.015	0.013	0.187	0.154
-2.25	0.106	0.091	0.555	0.510
-2.05	0.390	0.347	1.199	1.109
-1.85	1.019	0.941	2.164	2.155
-1.65	2.093	2.042	3.320	3.490
-1.45	3.506	3.576	4.685	5.096
-1.25	5.345	5.741	6.120	6.789
-1.05	7.181	7.967	7.684	8.666
-0.85	9.321	10.580	9.081	10.390
-0.65	11.060	12.880	10.340	12.030
-0.45	12.860	14.910	11.290	13.110
-0.25	14.050	16.420	11.980	13.950
-0.05	14.610	17.040	12.300	14.230
0.05	14.640	17.020	12.270	14.110
0.25	14.030	16.100	11.970	13.610
0.45	12.860	14.420	11.330	12.620
0.65	11.060	12.230	10.320	11.340
0.85	9.324	9.872	9.030	9.675
1.05	7.191	7.314	7.720	8.143
1.25	5.347	5.209	6.141	6.242
1.45	3.510	3.196	4.672	4.737
1.65	2.103	1.819	3.297	3.255
1.85	1.014	0.844	2.189	2.118
2.05	0.391	0.313	1.209	1.097
2.25	0.107	0.078	0.550	0.490
2.45	0.015	0.011	0.193	0.161

Table 12: The NLO exclusive $c\overline{c}$ and inclusive single charm y distributions for a proton beam of 800 GeV. The distributions for pp and pA interactions are both given. The per nucleon cross section is given for pA interactions. Recall that the intrinsic $\langle k_T^2 \rangle$ is 1 GeV^2 for pp interactions and 1.35 GeV^2 for pA interactions.

y (GeV)	$d\sigma_{c\overline{c}}/dy$ (μb) pp	pA	$d\sigma_c/dy$ (μb) pp	pA
-4.25	0.003	0.003	0.148	0.109
-3.95	0.125	0.105	0.939	0.772
-3.65	1.022	0.925	2.988	3.223
-3.35	3.398	3.263	7.240	7.515
-3.05	8.264	8.325	13.420	15.310
-2.75	15.050	16.570	20.550	22.350
-2.45	23.850	26.750	28.580	33.120
-2.15	33.690	38.640	36.600	43.300
-1.85	43.780	50.660	45.650	52.460
-1.55	54.080	63.880	53.330	61.470
-1.25	63.830	73.310	60.650	67.530
-0.95	69.960	78.450	65.320	70.720
-0.65	75.700	82.120	68.690	72.230
-0.35	79.700	82.990	71.950	72.470
-0.05	80.720	80.510	72.860	70.470
0.05	80.840	78.680	72.730	70.150
0.35	79.520	74.340	72.890	68.970
0.65	75.930	67.520	69.340	61.990
0.95	70.440	60.230	65.230	57.870
1.25	64.000	52.670	61.030	51.720
1.55	54.240	43.760	53.110	44.530
1.85	43.610	33.690	46.350	37.890
2.15	33.430	24.880	37.400	29.630
2.45	23.680	17.420	27.760	21.260
2.75	15.050	10.820	20.230	15.600
3.05	8.150	5.742	12.770	9.649
3.35	3.403	2.252	7.394	5.295
3.65	1.006	0.674	2.844	2.169
3.95	0.125	0.090	0.980	0.662
4.25	0.003	0.002	0.180	0.099

Table 13: The NLO exclusive $c\overline{c}$ and inclusive single charm y distributions for collisions at $\sqrt{s} = 200$ GeV. The distributions for pp and pA interactions are both given. The per nucleon cross section is given for pA interactions. Recall that the intrinsic $\langle k_T^2 \rangle$ is 1 GeV^2 for pp interactions and 1.35 GeV^2 for pA interactions.

	$d\sigma_{c\overline{c}}/dy$ (μb)		$d\sigma_c/dy$ (μb)	
y (GeV)	pp	pA	pp	pA
-4.85	117.0	128.4	186.8	200.4
-4.55	234.1	278.6	237.5	268.7
-4.25	369.4	428.5	331.2	346.9
-3.95	485.5	495.9	426.5	457.1
-3.65	532.9	586.9	522.0	522.1
-3.35	561.1	580.0	542.4	553.1
-3.05	594.1	586.8	590.5	564.2
-2.75	627.1	602.2	614.5	606.1
-2.45	650.1	616.5	650.6	565.6
-2.15	683.6	600.0	642.2	577.1
-1.85	685.5	587.8	681.9	582.8
-1.55	710.3	603.6	694.6	588.5
-1.25	705.9	618.8	672.0	578.2
-0.95	711.8	595.5	703.2	589.7
-0.65	735.9	611.1	736.7	617.2
-0.35	743.6	590.1	692.5	577.4
-0.05	720.6	556.8	716.7	560.5
0.05	715.6	548.0	721.1	557.8
0.35	741.4	564.0	699.3	552.3
0.65	744.0	567.4	706.2	555.3
0.95	708.6	541.4	701.5	530.4
1.25	702.3	546.4	704.2	520.6
1.55	713.9	506.9	664.2	497.5
1.85	689.1	482.1	678.2	477.1
2.15	687.6	476.7	639.9	462.9
2.45	651.9	470.5	620.5	447.6
2.75	625.8	437.6	606.6	422.2
3.05	589.7	412.5	591.6	415.5
3.35	564.0	384.7	555.1	388.1
3.65	532.9	379.3	516.0	350.9
3.95	479.2	304.0	430.2	297.4
4.25	371.3	257.4	357.9	226.2
4.55	230.3	153.8	226.4	164.3
4.85	112.1	69.4	193.4	104.4

Table 14: The NLO exclusive $c\overline{c}$ and inclusive single charm y distributions for collisions at $\sqrt{s} = 5.5$ TeV. The distributions for pp and pA interactions are both given. The per nucleon cross section is given for pA interactions. Recall that the intrinsic $\langle k_T^2 \rangle$ is 1 GeV^2 for pp interactions and 1.35 GeV^2 for pA interactions.

	$d\sigma_{b\bar{b}}/dy$ (nb)		$d\sigma_b/dy$ (nb)	
y (GeV)	pp	pA	pp	pA
-2.65	0.8	0.7	14.1	12.1
-2.45	4.8	4.2	33.0	26.6
-2.25	16.6	14.3	61.1	59.2
-2.05	41.1	38.3	103.7	100.0
-1.85	82.8	80.2	150.0	154.8
-1.65	138.2	140.8	203.4	220.3
-1.45	213.3	222.4	262.8	287.3
-1.25	289.1	313.4	323.3	361.1
-1.05	382.7	417.3	383.9	432.0
-0.85	463.7	518.7	443.2	489.1
-0.65	543.8	609.8	482.7	548.9
-0.45	606.8	692.5	520.3	589.4
-0.25	651.4	739.2	547.5	615.2
-0.05	674.7	764.2	555.3	617.2
0.05	674.1	762.7	553.5	615.6
0.25	650.8	726.9	545.0	606.1
0.45	607.3	671.0	520.1	570.5
0.65	543.3	582.9	481.7	522.5
0.85	463.9	491.0	440.1	466.3
1.05	383.1	391.0	387.5	406.7
1.25	289.0	291.1	323.5	338.0
1.45	213.3	205.7	264.0	269.3
1.65	138.7	130.4	205.7	210.2
1.85	82.9	75.3	148.6	147.1
2.05	41.2	36.4	102.1	99.0
2.25	16.6	13.7	59.9	58.3
2.45	4.8	4.0	31.3	30.7
2.65	0.8	0.6	13.5	12.8

Table 15: The NLO exclusive $b\bar{b}$ and inclusive single bottom y distributions for collisions at $\sqrt{s} = 200$ GeV. The distributions for pp and pA interactions are both given. The per nucleon cross section is given for pA interactions. Recall that the intrinsic $\langle k_T^2 \rangle$ is 1 GeV^2 for pp interactions and 2.57 GeV^2 for pA interactions.

y (GeV)	$d\sigma_{b\overline{b}}/dy$ (μb)		$d\sigma_b/dy$ (μb)	
	pp	pA	pp	pA
-4.85	1.811	1.831	3.012	3.239
-4.55	2.940	3.117	4.652	5.331
-4.25	5.035	5.625	6.328	7.331
-3.95	7.070	7.946	8.606	9.596
-3.65	9.872	11.200	10.500	12.110
-3.35	12.260	13.800	12.780	14.330
-3.05	14.330	16.330	14.770	16.100
-2.75	17.350	19.110	16.950	18.230
-2.45	19.100	21.030	18.730	20.040
-2.15	21.350	22.880	20.070	20.650
-1.85	22.890	23.940	21.300	22.290
-1.55	24.010	23.790	23.250	22.740
-1.25	25.320	24.830	24.040	23.790
-0.95	26.500	25.570	25.360	23.960
-0.65	26.660	25.160	25.380	24.050
-0.35	27.460	25.330	25.480	23.380
-0.05	27.050	24.680	26.170	23.810
0.05	27.010	24.500	25.790	23.920
0.35	27.330	24.130	25.320	22.810
0.65	26.660	23.340	25.380	21.990
0.95	26.460	22.770	25.480	21.810
1.25	25.310	21.310	23.830	20.230
1.55	24.080	19.630	22.540	19.050
1.85	22.830	19.060	21.370	17.920
2.15	21.320	17.380	20.000	16.690
2.45	19.100	15.280	18.770	15.570
2.75	17.360	13.580	17.320	13.780
3.05	14.410	11.260	14.670	11.580
3.35	12.140	9.320	12.740	10.040
3.65	9.831	7.393	10.430	7.929
3.95	7.049	5.294	8.431	6.380
4.25	5.017	3.721	6.190	4.889
4.55	2.925	2.147	4.660	3.450
4.85	1.797	1.290	3.080	2.222

Table 16: The NLO exclusive $b\overline{b}$ and inclusive single bottom y distributions for collisions at $\sqrt{s} = 5.5$ TeV. The distributions for pp and pA interactions are both given. The per nucleon cross section is given for pA interactions. Recall that the intrinsic $\langle k_T^2 \rangle$ is 1 GeV^2 for pp interactions and 2.57 GeV^2 for pA interactions.